Stieltjesweg 1
2628 CK Delft
P.O. Box 155
2600 AD Delft
The Netherlands

www.tno.nl

T +31 88 866 20 00
F +31 88 866 06 30

TNO report | Bachelor Thesis

Detection of corrosion in the circumferential direction of pipelines using highly dispersive Lamb waves

Author	Mick Hsu
Institution	The Hague University
Coach	A. Volker
Internship coaches	R. Buning
	K. Bol
External examiner	H. van den Brom

Date of submission 4 June 2015

Abstract

Corrosion inside pipelines caused by salt water is a major problem for maintenance in the oil and gas industry. Corrosion reduces the wall thickness of the pipe. There is a need to determine the severity of corrosion inside a section of pipeline to decide if it needs replacement. A Non-Destructive Testing (NDT) technique using ultrasonic guided waves is one of the ways to accomplish this.

Guided waves in plates are called Lamb waves. These waves are guided by the pipe wall and can travel along the circumference. This allows a measuring unit consisting of a source and receiver on top of the pipe to detect corrosion at the bottom of the pipe without requiring direct access to it. The speed of the wave is dependent of its frequency and wall thickness of the medium. By sending a short sine burst and comparing the arrival times of this wavelet the wall thickness can be measured.

TNO wants to investigate the use Electro Magnetic Acoustic Transducers (EMATs) as the source and receiver of Lamb waves for sizing corrosion in pipes. EMATs do not require mechanical contact with the pipe wall to excite or detect Lamb waves. This is an advantage over the widely used piezoelectric transducers. The goal is to make a wall thickness profile of a section of pipe with defects.

The distance between the source and receiver EMAT is important to consider. Because of the geometry of the pipe circumference and different wave modes with different speeds, the wavelets might overlap at the receiver. Using a Finite Difference (FD) simulation a range of acceptable source receiver distances is identified.

Measurements have been carried out on three pipes: one with artificial defects (TNO pipe) and two with real corrosion spots (Shell and Dow pipe). Using the TNO pipe a measuring method is established. Measurements have been done with different centre frequencies of the wavelet. A centre frequency of 180 kHz was chosen as the optimal centre frequency. Measurements comparing sections of the pipe with mill scale and without mill scale reveal that magnetostriction inside the mill scale increases the overall amplitude of the signal. It especially increases the amplitude of the A0 mode.

A section of the TNO pipe has been measured and the results are compared to known defect locations. The defect locations are able to be identified from the measurements. A wall thickness profile has not been made but an approximation of the shape of the wall thickness profile has been acquired.

The approximated wall thickness profile of the Shell pipe has been compared to the wall thickness profile acquired from previous measurements. The general shape corresponds and the primary defect location is identifiable. The measurements on the Dow pipe underestimate the relative depth of the pitting corrosion. This might be caused by the small size of the pitting.

Contents

1 Introduction

In the oil and gas industry the proper maintenance of pipelines is of great importance to safety. The structural integrity of a pipe might be compromised when there is a large amount of corrosion. It is therefore important to inspect the pipe wall on a regular basis. With the use of non-destructive testing techniques that do not interfere with the operation of the pipeline, sections of the pipe wall can be inspected. There are two possible directions along a pipeline to examine: along the length of the pipeline and along the circumference. The former is mainly used as a way to locate corrosion areas. The circumferential examination is used for a more detailed examination to measure the severity of the corrosion on a section of pipe. This is done by measuring the wall thickness loss caused by corrosion to decide if the corroded section needs a replacement.

Ultrasonic testing is one of the primary techniques used to inspect wall thickness loss in pipelines. Conventional ultrasonic testing relies on sending a sound wave perpendicular to the surface of the pipe and analysing the attenuation or reflection of the wave. The disadvantage of this technique is that only a small surface area can be inspected at a time and it is not possible to measure sections of the pipe that are obstructed. A more recent technique is the use of ultrasonic guided waves. Guided waves propagate parallel to the surface of the pipe, this way the entire circumference of a section of pipe can be measured in one measurement. This technique also requires only small portion of the pipe wall to be exposed. This is helpful when a section of the pipe is inaccessible such as when covered by a pipe support or buried underground. Guided waves are usually generated by piezoelectric transducers, these require direct contact with the material via a couplant. TNO has developed electromagnetic acoustic transducers (EMAT) to generate guided waves for circumferential pipeline inspection. EMATs do not require direct contact with the material. This makes them applicable in a variety of conditions where piezoelectric transducers cannot be used, for example when pipe wall temperatures are very high. Previous research has been done by TNO on EMAT design[7] and corrosion detection in plates using Lamb waves[8].

In this thesis the possibility of using Lamb waves excited by EMATs to size corrosion in piping is investigated. First the theory of Lamb waves and the principle of corrosion detection are studied (Chapter 2). Then simulations are made using Matlab to study the behaviour of the waves in cylinders (Chapter 3). Measurements were done on a pipe with artificial defects to verify the simulation results and to establish a method to measure wall thickness loss (Chapter 4). Finally three pipes have been measured from which two had real corrosion spots to acquire an approximation of the wall thickness profile along the length of the pipes (Chapter 5).

2 Corrosion detection with Lamb waves

A major hazard to the structural integrity of pipelines is the formation of corrosion inside the pipe and the resulting wall thickness loss. It is therefore important for maintaining the pipeline that the location and amount of corrosion can be measured. In this thesis the focus will be on an acoustic Non-Destructive Testing (NDT) technique using guided waves to size the corrosion spot along the circumference of the pipe. This technique uses ultrasonic guided waves, their speed depends on their frequency and thickness of the medium. The latter characteristic can be used to gauge wall thickness loss due to corrosion. Electro-Magnetic Acoustic Transducers (EMATs) are also discussed, they are used to excite and detect the ultrasonic waves.

2.1 Waves for ultrasonic testing

Non-Destructive Testing is a way to inspect samples without causing damage to it. There are many different approaches to NDT but in this thesis it will be limited to using ultrasonic testing techniques for corrosion detection in pipelines.
Ultrasonic testing works by using an ultrasonic source and a detector to analyse either the transmitted or reflected signal (echo) through a sample. This way information can be derived about possible inhomogeneity's or defects in the sample.

Waves have two ways of displacement: longitudinal and transversal. Longitudinal waves have a displacement parallel to the direction of propagation while transversal waves, also known as shear waves, displace perpendicular to the direction of propagation. Most waves are a superposition of these two wave types. Different materials have different properties for the propagation speed in longitudinal and transversal direction, with the longitudinal direction being faster.

Elastic waves can be classified into two categories: bulk waves and guided waves. Bulk waves are waves that propagate in (semi-)infinite media. They travel in the bulk of a material and their wavelengths are small compared to the thickness of the medium. Guided waves propagate in media where its wavelength is large compared to the thickness, they are guided by the boundary of a sample.

Bulk waves as well as guided waves are being used in acoustic NDT of pipes.
With conventional ultrasonic testing using bulk waves only a small section of pipe can be inspected at a time. The ultrasonic source must move over the surface of the pipe to measure it. Guided waves on the other hand travel through the entire wall thickness of the pipe and thus travel along the circumference of the pipe (Figure 1). This enables faster measurements and doesn't require the whole pipe to be exposed. This technique is able to detect corrosion on the inside as well as on the outside of the pipe. This is helpful when a section of the pipe is inaccessible such as when covered by a pipe support or buried underground. Corrosion also tends to occur at the bottom of a pipe because any remaining salt water gathers there.

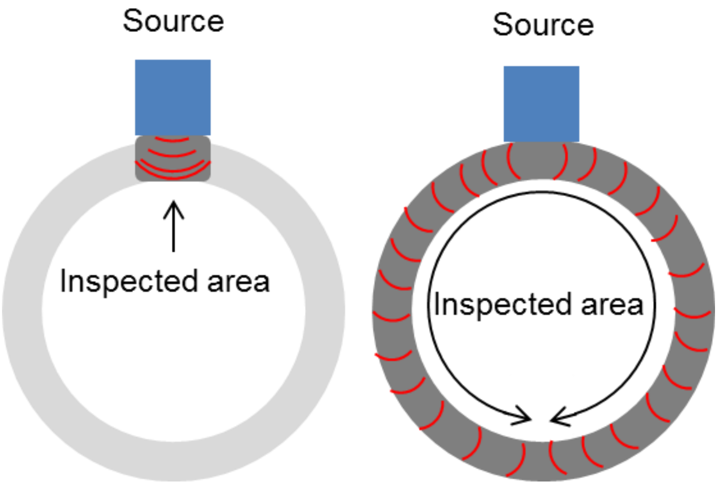

Figure 1: An illustration of the difference between conventional ultrasonic testing and guided wave testing. The grey bar represents the circumference of the pipe wall.

2.2 Lamb waves

The English mathematician Horace Lamb was the first to describe wave propagation in plates, these plate waves are therefore also known as Lamb waves. Lamb waves are guided waves that exist in plate-shaped media, their wavelength is in the order of magnitude as the thickness of the plate. The upper and lower surface of the plate provides a boundary that guides the waves. Lamb waves have both a longitudinal and transversal velocity component.

Lamb waves are described with the Rayleigh-Lamb frequency equations[2, 3] (Equation 1 & 2), these equations reveal that there are two families of modes present within a plate: one symmetric and one antisymmetric with respect to the midplane of the plate (Figure 2). c_L and c_T are material properties, for all solids the longitudinal velocity is higher than the shear velocity. An important characteristic of Lamb waves is that they are dispersive, that means their speed is dependent of frequency. From the equations it is also shown that the speed is dependent of the thickness of the plate, this property is used in pipe wall inspection.

$$\frac{\tan(qh)}{\tan(ph)} = -\frac{4k^2 pq}{(q^2 - k^2)^2} \quad \text{for symmetric modes} \qquad (1)$$

$$\frac{\tan(qh)}{\tan(ph)} = -\frac{(q^2 - k^2)^2}{4k^2 pq} \quad \text{for antisymmetric modes} \qquad (2)$$

With p and q given by: $p^2 = \left(\frac{\omega}{c_L}\right)^2 - k^2$ and $q^2 = \left(\frac{\omega}{c_T}\right)^2 - k^2$

where:
k = Wavenumber (m^{-1})
ω = Circular frequency (s^{-1})
h = Half-thickness of the plate (m)
c_L = Velocity in longitudinal direction (m/s)
c_T = Velocity in transversal (shear) direction (m/s)

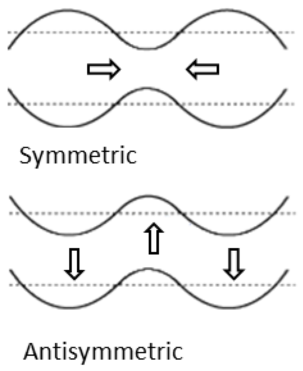

Figure 2: Schematic representation of the symmetric and antisymmetric Lamb wave modes. The dotted line represents the plate with the vertical axis being the thickness of the plate, the unbroken lines represents the wave. [4]

The Rayleigh-Lamb frequency equations only describe particle motion in waves in the x-direction (direction of wave propagation) and z-direction (direction of the plate normal). Waves displacing in the y-direction are called shear horizontal (SH) waves and exhibit different characteristics than the standard Lamb waves. SH waves in the frequency range used in this research cannot be used for corrosion detection because they are not dispersive, thus they are not sensitive to wall thickness change. They will not be discussed any further.

2.3 Phase and group velocity

The concepts of phase velocity and group velocity are important for understanding acoustic wave physics. The phase velocity is the speed of which any fixed phase of a wave is moving in space (Equation 3).

$$c_p = \frac{\omega}{k} \tag{3}$$

Group velocity is the propagation velocity a group of waves with a small difference in wavelength (Equation 4). It can be considered as the speed of a wave packet or wavelet. Often this is the speed at which energy and information moves through a medium (Figure 3).

$$c_g = \frac{\Delta\omega}{\Delta k} \tag{4}$$

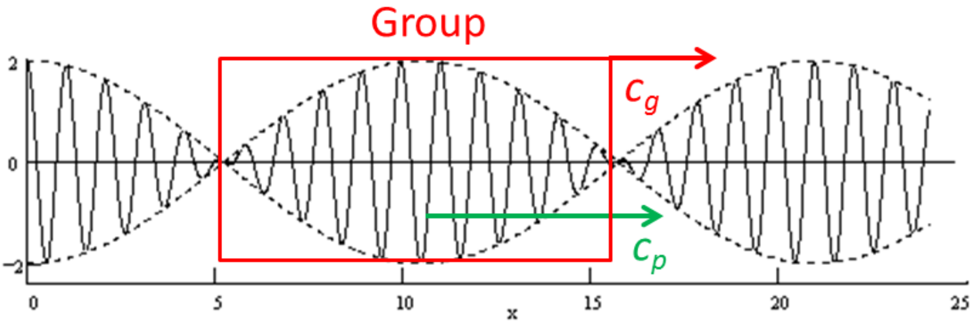

Figure 3: Example of group velocity and phase velocity. [5]

The frequencies of the waves in a group are in a band around its centre frequency, in other words the frequency of the individual waves in a group differs slightly. Because of the frequency dependence of the phase velocity, the individual waves in a group will experience dispersion. The wave group will become longer along the direction of propagation as the waves travels further. For the understanding of wave behaviour it is important to know the exact relation between c_p/c_g and the frequency.

For Lamb waves the group velocity is given by Equation 5: [2]

$$c_g = c_p^2 \left(c_p - \omega \frac{dc_p}{d\omega} \right)^{-1} \tag{5}$$

2.4 Dispersion curves

Dispersion curves graphically represent the relation between the phase or group velocity as function of the frequency. Equations 1 and 2 are also known as dispersion relations and can be rewritten and solved numerically to obtain the dispersion curves for Lamb waves in different materials. An example is shown for Lamb waves in an aluminium plate in Figure 4.

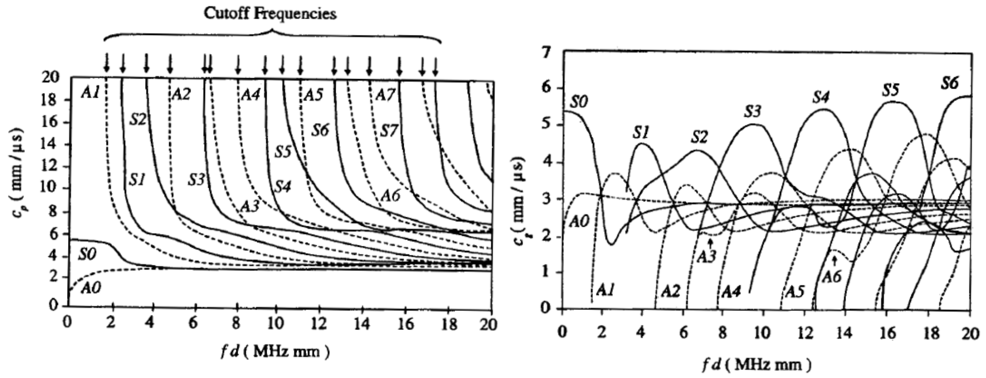

Figure 4: Dispersion curves for the phase velocity (left) and group velocity (right) as function of frequency-thickness (*fd*) product for an aluminium plate. The solid lines represent the S modes and the dashed lines the A modes.[1]

As is common, the phase velocity and group velocity is plotted against the frequency-thickness (*fd*) product. Sometimes they are plotted against the wavenumber- half-thickness product ($k_t d$) which relates to the *fd* with Equation 6. [2]

$$fd = \frac{2 \cdot k_t d \cdot c_s}{2\pi} \tag{6}$$

Where:
fd = frequency-thickness product (Hz·m)
$k_t d$= wavenumber-half-thickness product (-)
c_s = Velocity in transversal (shear) direction (m/s)

The letter S and A denote the symmetric and antisymmetric modes respectively, the number denotes the order of the mode. As seen from Figure 4 the zero-order modes exist across all frequencies while the higher order modes have a cut-off frequency. Also note that the symmetric modes are usually faster than the antisymmetric modes and the S0 and A0 mode converge at higher *fd* values.
A relation between the speed of the wave and the thickness of the plate can be deduced from the dispersion curves if the frequency remains constant. This can be used to examine thickness deviations in the plate medium. It is useful to excite a limited number of modes as the signal at the detector can become complex because of overlapping signals when using a large frequency spread.

Another consideration is the individual characteristics of the different modes. For example some waves are more sensitive for defects at the surface of a plate. The symmetric modes of Lamb waves are commonly referred to as compressional modes and the antisymmetric modes as flexural modes. However the symmetric mode does not only have particle displacement in the longitudinal direction and the antisymmetric mode doesn't consist purely of transversal motion. The wave structure of each mode changes with *fd* product. For example if the *fd* increases for the S0 mode the in-plane (longitudinal) displacement goes along the thickness of the plate from a uniform distribution (Figure 5a) to a distribution more concentrated in the middle (Figure 5f). The out-of-plane displacement becomes larger at the outer regions of the plate while the centre stays zero.

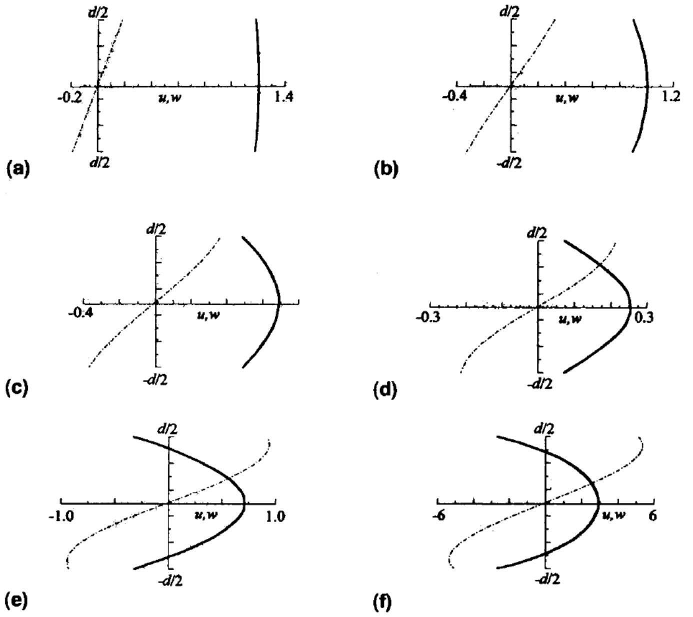

Figure 5: Wave structure of the S0 mode for different *fd* values in an aluminium plate. The solid line represents in-plane and the dashed line the out-of-plane displacement profile along the thickness of the plate. [1]

2.5 EMAT

An Electro-Magnetic Acoustic Transducer also known as EMAT is a type of transducer that relies on electromagnetic interaction with a sample to excite an acoustic wave. EMATs require no direct contact with the sample unlike the more traditional piezo-electric transducer which needs a couplant. This makes them more versatile in NDT applications. EMATs can be used as a source and as a detector of acoustic waves.

The basic components of an EMAT are a permanent- or electromagnet and a coil. EMATs use two mechanisms to generate acoustic waves: the Lorentz force and magnetostriction in ferromagnetic materials. Ferromagnetic materials have an internal structure divided into domains, each with a different magnetic polarization. When a magnetic field is applied the domains will rearrange to align itself with the field, this causes a particle displacement in the material and thus creates a wave if the magnetic field alternates. The working mechanism by the Lorentz force will be discussed more in-depth as it is the dominant force used in this study and is also applicable to non-ferromagnetic materials.

When an alternating current runs through the coil it will induce an eddy current at the surface of the sample in opposite direction. The frequency of the current is the frequency of the excited wave. The type of coil dictates what kind of wave is excited, for Lamb waves a meander coil design is used (Figure 6). The spacing between the wires is equal to half the wavelength of the excited wave, thus each turn is equivalent to the wavelength. This means that the design of the coil determines which wave frequencies are primarily excited. This also allows for exciting one wave mode more than another at certain frequencies.

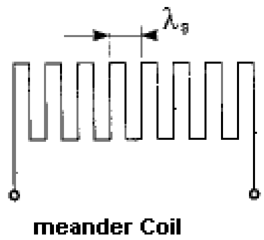

Figure 6: An example of an 8 turn meander coil configuration.[6]

Perpendicular to the current direction and magnetic field created by the magnet a Lorentz force inside the sample will be generated. The Lorentz force displaces particles in a longitudinal direction and generates a wave inside the sample (Figure 7). Because of the current flowing through the coil and eddy currents inside the plate a repellent force is created between the two. This creates transversal waves.

In a similar way the EMAT is also able to function as a detector: particle displacement in the sample together with the magnetic field creates a current in the sample and induces a current in the coil of the EMAT.

Another aspect of EMATs is the distance between the sample and the EMAT this is called 'lift off'. The closer the EMAT is to the sample the more energy of the acoustic wave is transferred. The typical lift off is in the order of millimetres to micrometres.[7]

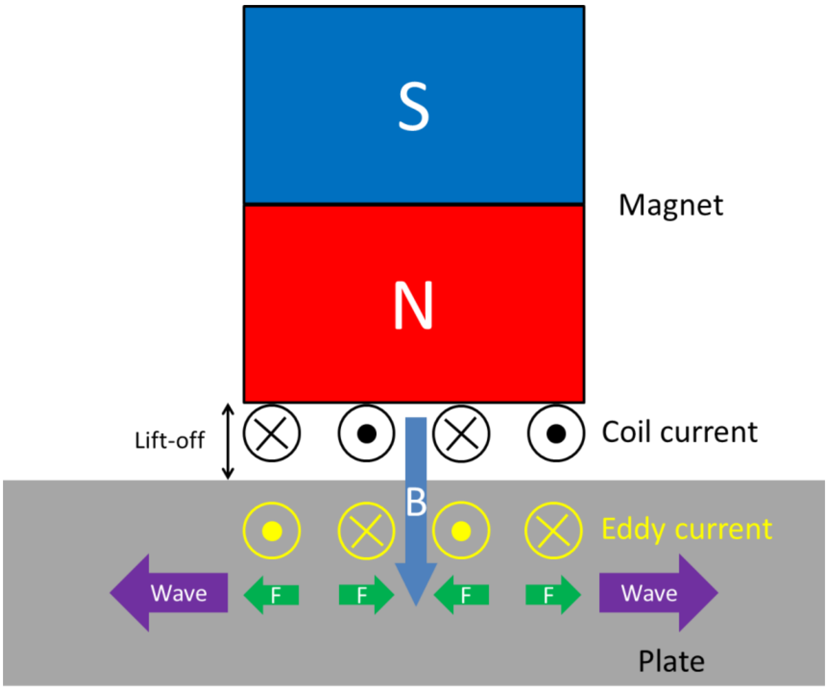

Figure 7: Schematic overview of how an EMAT creates a wave using the Lorentz force.[9]

2.6 Wall thickness inspection

Until now Lamb waves have been described as guided waves in flat plates. The behaviour of Lamb waves in hollow cylinders, such as pipes, is very similar to that in flat plates because the pipe wall can be thought of as a folded plate. In a hollow cylinder there are two kinds of Lamb waves: waves that propagate in the circumferential direction of the pipe and those that propagate in the length of the pipe.

The circumferential directional waves are very similar to the Lamb waves in plates. The dispersion curves are therefore similar with the two most significant differences being that for low *fd* values they differ and for high *fd* values the S0 and A0 mode doesn't converge. The waves travelling along the length of the pipe are useful in determining which section along the pipeline might have corrosion spots. Longitudinal waves are beyond the scope of this thesis and won't be discussed any further.

A typical inspection setup would consist of two EMATs on a section of pipe. One EMAT is the source and the other the receiver, they are set apart at a set distance from each other (Figure 8). A power amplifier connected to the coil of the source EMAT emits a current in the form of a sine pulse. The EMAT excites the wavelet in the pipe wall, the wavelet then travels in both directions along the circumference. The pulses are registered when they pass by the receiver. The time it took for the wavelet to reach the receiver is compared to the time it would take if there was no wall thickness loss. The difference in time is a measure of wall thickness loss.

Because the source and receiver are not on the same position multiple wavelets might pass the receiver at the same time because of path length difference. Furthermore, different wave modes travel at different speeds which also can lead to cluttering of the signal. If a signal is too complex it cannot be used for wall thickness inspection. By using low *fd* values the higher order modes are omitted. Then, only two wave modes remain the S0 and A0. A particular source receiver distance of which the two modes do not overlap at the receiver has to be used. Furthermore, one of the modes can be suppressed with the design of the EMAT coil and choice of centre frequency.

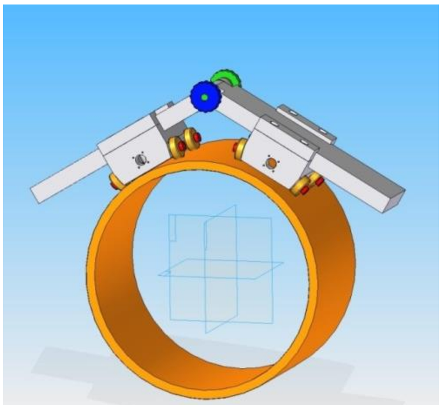

Figure 8: A conceptual representation of the measuring setup. Two EMATs, one transmitter and one receiver, are secured with screws on two beams joined with a hinge. The EMATs are on wheels so it can move along the pipe.

3 Simulations

To get a better understanding of Lamb wave behaviour some simulations have been carried out with models made in Matlab. Their results have been analysed to predict experimental results. Furthermore a Matlab function has been created to assist in analysing experimental results. The phase and group velocity of the S0 and A0 modes have also been calculated with Matlab.

3.1 Dispersion curves calculation

Equations 1 and 2 have been numerically solved for the S0 and A0 modes for 11 different Poisson ratios between 0.250 and 0.350. The calculated dispersion curves for the phase speed are independent of shear velocity and are stored together with the $k_t d$ values. From these data files the phase velocity of the S0 and A0 modes have been calculated by multiplying the numerical data with the shear velocity of the desired medium material. The dispersion curves for different Poisson ratios can be obtained by interpolating the data files. In Equation 7 the group velocity is calculated by using $\omega = 2\pi f$ to rewrite Equation 5:

$$c_g = c_p^2 \left(c_p - (fd) \frac{dc_p}{d(fd)} \right)^{-1} \tag{7}$$

In Figure 9 the phase velocity of the S0 and A0 modes have been plotted for steel with a shear velocity of 3100 m/s. The group velocity has also been calculated and plotted as a function of *fd* calculated from the $k_t d$ values using Equation 6.

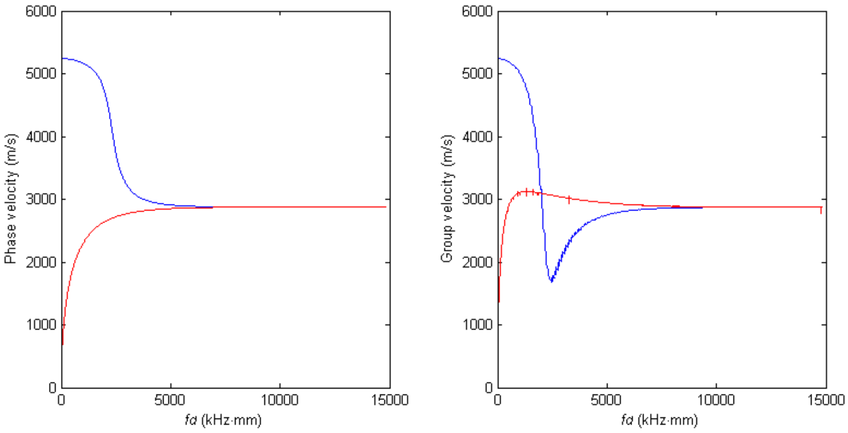

Figure 9: Dispersion curve of the S0 (blue) and A0 (red) mode for a Poisson ratio of 0.300. The phase velocity is shown on the left and the group velocity on the right. The spikes in the group velocity are caused by the amplification of noise when taking the derivative of the phase velocity.

A Matlab function has been made to receive an *fd* as input and to output the phase and group speed of the S0 and A0 mode. The values between the data points of the dispersion curves are linearly interpolated.

3.2 2D cylinder finite difference simulation

When the transmitter creates the ultrasonic wave for the measurement some undesired waves of different frequency and mode than the dominant wave will also appear. Choosing the right distance between the source and receiver is important because otherwise the detected signal may be cluttered by the undesirable waves. To find that distance a Finite Difference (FD) model of a 2D cross-section of a pipe in Matlab has been used. It simulates Lamb wave propagation and detected signal at different source receiver distances. The simulation was made before this research and will be used for verification of a simulation made by the author (Paragraph 3.3).

3.2.1 Finite difference modelling

A model consists of a domain with certain geometry. The domain can be divided into smaller elements. Partial differential equations describe the physical characteristics of each element based on the surrounding elements. Thus a model consists of a set of partial differential equations that has to be solved. These equations cannot be solved analytically so a numerical method has to be used. The finite difference method is a numerical method to solve differential equations by approximating them with difference equations using the Taylor series. By solving the system of equations, values for the physical characteristics can be found.

3.2.2 The model

The geometry of the model consists of a hollow circle. At one section at the outer wall of the circle a wave source is positioned. The source consists of four points equally spaced along the outer wall, these represent the EMAT coil. The source emits a sine wave pulse, in the direction of the circumference so it will mainly excite the S0 mode. The displacement of the wavelet is calculated while it propagates in the wall. The amplitude of the wave is measured along the entire circumference. The dimensions of the pipe used in the simulation resembled the experimental setup: the inner radius is 0.130 m, the outer radius is 0.138 m. The pipe is made of steel: the longitudinal and shear velocity of the wall are 5950 m/s and 3100 m/s respectively and it has a density of 7800 kg/m^3. The centre frequency of the wavelet is 150 kHz and uses three phase cycles.

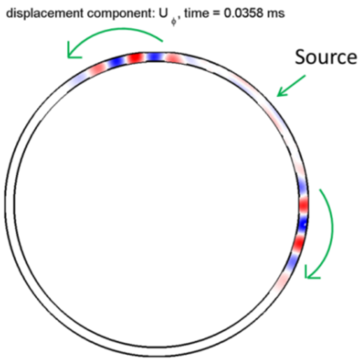

Figure 10: Geometry of the 2D cylinder simulation. The red and blue colours represent positive and negative displacement respectively in the longitudinal direction of the traveling wavelet.

The EMAT coil has four turns with a 1.72 cm distance between them. This optimizes the EMAT for exciting wavelengths of 3.44 cm. In Figure 11 the dispersion curve is given for the S0 and A0 mode. If a line of constant wavelength of 3.44 cm is plotted in the dispersion curve it can be seen that it intersects the S0 curve at 150 kHz. This means that around this frequency the EMAT will excite this mode the best. On the other hand the line intersects the A0 curve at 50 kHz. This means that when using a centre frequency of 150 kHz the A0 mode will be excited with lower amplitude than the S0 mode. Also note that when using higher frequencies the slope of the S0 curve increases and thus the sensitivity.

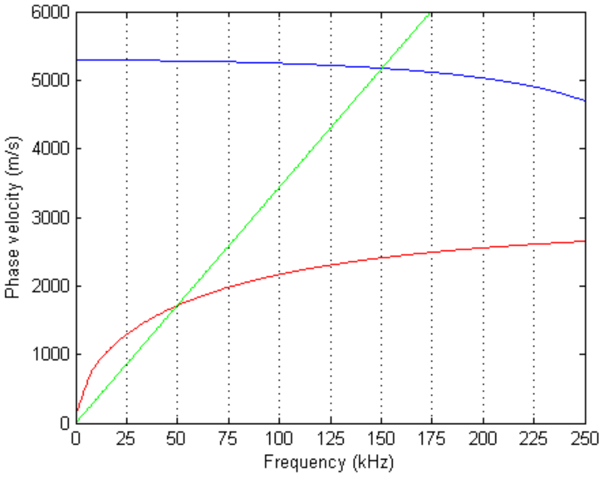

Figure 11: A dispersion curve for a wall thickness of 8 mm and Poisson ratio of 0.314. The S0 (blue) and A0 (red) mode is shown along with a line of constant wavelength of 3.44 cm (green).

3.2.3 FD simulation results

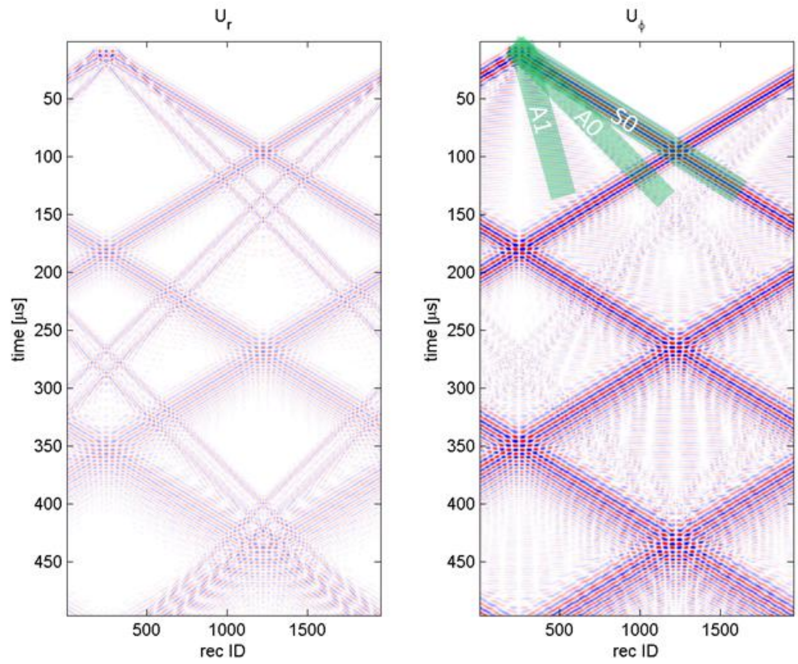

Figure 12: Overview of the results from a simulation. Displayed left is the radial (transversal) displacement and right the angular (longitudinal) displacement. The x axis represents position along the circumference, the source is approximately at rec ID 250. The couloirs represent the amplitude of the wave: red is positive and blue is negative. The green area's represent the starting points of the S0, A0 and A1 modes.

In Figure 12 the results of a simulation using the model is displayed. The x axis represents a position along the circumference of the cylinder, the circumference is 0.87 m. The y axis represents time. The source is at approximately position 250, at time 0 it emits a sine pulse. The wavelet travels along the circumference and after 50 µs three modes are distinguishable: S0, A0 and A1. The beginnings of these modes are highlighted in green. The S0 is the top most horizontal bold line, it is the fastest of all the modes. The A0 is the line under the S0, it is slightly slower, the A0 can be seen more clearly in the left figure because its displacement is highest in the transversal direction. The A1 is the slowest of them all and is going almost vertical in the figure. Notice how dispersion causes the wavelet to become wider in the y direction as it travels. Also note that the simulated amplitudes of the different modes are not representative of real measurements.

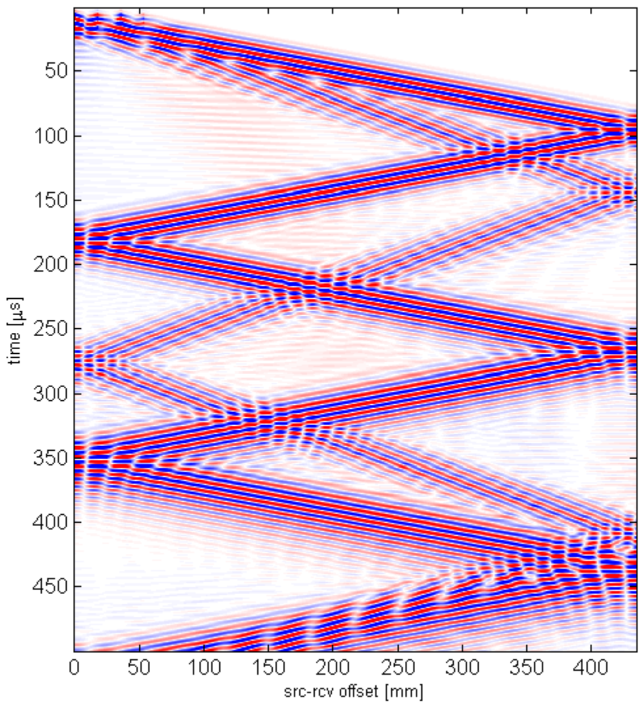

Figure 13: Longitudinal displacement of the S0 (darker) and A0 (lighter) modes in time along different source to receiver distances.

In Figure 13 the longitudinal component of the S0 and A0 are plotted together to mimic the EMAT response. The x axis represents the source to receiver distance, thus a vertical slice of the image gives the receiver response at a certain source receiver distance as function of time. It is important that the different wavelet paths in the figure remain separate so they can be analysed individually. The region between 200 mm and 300 mm are therefore suitable source receiver distances.

In Figure 14 a vertical slice from Figure 13 at the 205 mm position is shown. This signal is similar to a measured signal. The S0 mode has the highest amplitude. The first arrival took the most direct route with a path length equal to the Source and Receiver distance (SR), see Figure 15. The second S0 arrival travelled along the opposite side of the pipe, its path length is the difference between circumference and SR distance. The third S0 arrival has a path length of the sum of the circumference and SR distance. This means that in practice the first arrival cannot be used to detect corrosion because it has not passed through it. The second and third arrivals have passed the corrosion once. The fourth and fifth arrivals have passed the corrosion twice. Note that the amplitude of the signal is not used to detect corrosion. The phase difference between a signal that passes through a defect and a signal that did not, yields information about the defect size and depth.

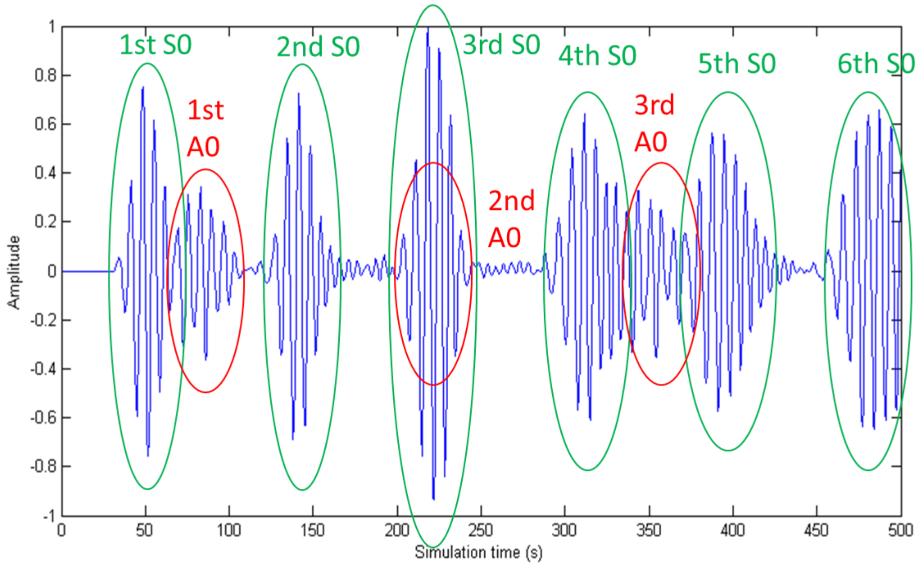

Figure 14: A vertical slice from Figure 13 at a source receiver distance of 205 mm.

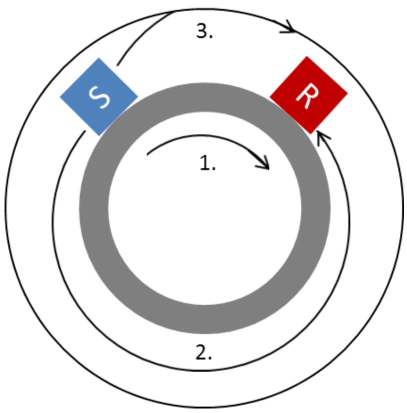

Figure 15: Schematic representation of the different paths of the wavelet. Path one is the shortest route between source and receiver. Path two propagates opposite of path one. Path three is the longest route.

3.3 Semi analytic Lamb wave simulation

A simulation has been performed to predict the wave shape of the S0 and A0 modes at a certain position in the pipe wall. It takes into account the wall thickness profile and EMAT coil. This is already possible using the FD simulation however by using this simulation it is possible to calculate it much faster. This is required to run an inversion on the data. Measurement data is used as input and the script calculates a wall thickness profile. The inversion itself is however beyond the scope of the research. The semi analytic Lamb wave simulation uses a Fourier transform to shift the wavelet and therefore it will be referred to as the FT simulation. The results of the FT simulation will be compared to the FD simulation and measurements.

3.3.1 The model

The geometry is defined as a one dimensional profile, this profile represents the circumference of a pipe. The profile is divided into elements of equal length *dx*, each element has a wall thickness value. A source wavelet is defined as starting wavelet. The goal is to calculate the shape of the wavelet at a position along the circumference taking into account the dispersion effects so the resulting wavelet is representative of an experimentally measured wavelet. This is done by phase shifting each frequency of the wavelet with a time τ.

The phase speed at every element for every frequency of the wavelet is calculated from the dispersion curves according to the wall thickness of each element.
By dividing *dx* by the associated phase speed the time that takes for the wavelet to pass the element can be found (Equation 8). By taking the sum of the number of elements desired to reach a certain position along the circumference the total time to shift can be calculated (Figure 16).

$$\frac{dx}{c_p} = d\tau \tag{8}$$

Where:
τ = Travel time (s)

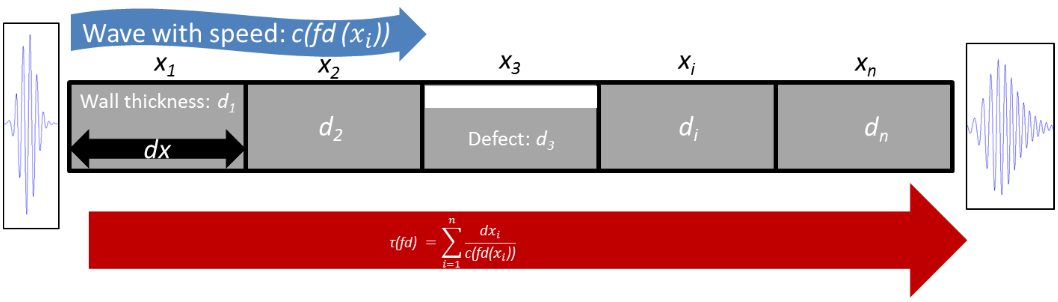

Figure 16: Schematic representation of phase shifting a wavelet in the FT simulation.

This process is done for the S0 and A0 modes. To shift the wavelet in time the time shift property of the Fourier transform is used (Equation 9). A Fourier transform is performed on the wavelet. In the Fourier space it is multiplied with the phase shift operator and then transformed back into the time domain.

$$F\{s(t-\tau)\} = S(f) \cdot e^{-i\omega\tau} \tag{9}$$

Where:
s = Wave function (-)
S = Fourier transform of wave function (-)

The FT simulation simulates the behaviour of a receiver EMAT by calculating the measured wave at four coil positions around a central position given by the source-receiver distance. The distance between these points is equal to the distance between the coil turns of the EMAT. The final signal is the summation of the waves at these points taking into account the current direction in each turn (Figure 17). The FT simulation also corrects for the fact that the wavelet travels along the central axis of the pipe wall instead of the surface. The final goal of this simulation was to invert it so it takes a measurement signal as input and fits a wall thickness profile to the data. This has not been done due to lack of time.

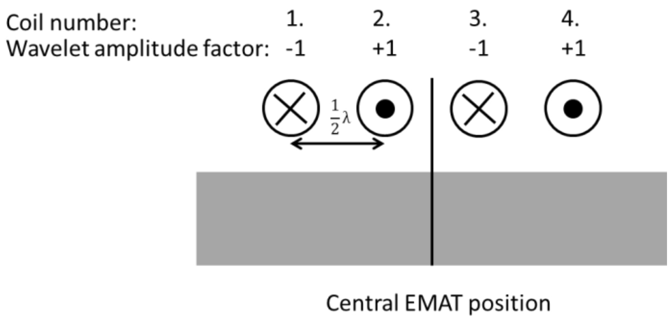

Figure 17: Schematic overview of the FT simulation simulates an EMAT receiver. The receiver signal is calculated at four positions representing the EMAT coils. They are then summed taking into account the current direction in the coils.

3.3.2 Ft simulation results

Using the same settings as the FD simulation a simulation has been done to verify the results of the FT simulation. The main parameters are: 150 kHz centre frequency, 278 ns time step, 138 mm outer pipe radius, 8 mm nominal wall thickness, 205 mm source receiver offset and 0.1 mm position step.
Three revolutions along either side of the source have been simulated, the resulting S0 and A0 modes are plotted in Figure 18. It can be seen that the A0 mode has overlap with some of the S0 wavelets.

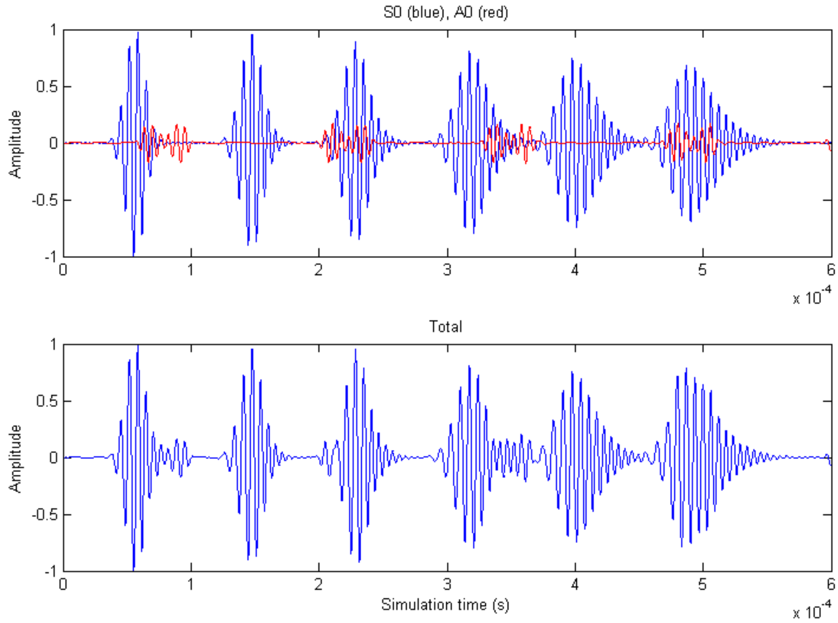

Figure 18: FT simulation result with a 150 kHz centre frequency and 205 mm source receiver distance. On top the S0 and A0 modes are plotted separately in blue and red respectively. At the bottom the sum of both waves is shown.

In Figure 19 the FT simulation is compared to the FD simulation. The position of the wavelets are aligned, there is some difference in the amplitude at the end of each S0 wavelet probably caused by a difference in frequency spectrum. Also the amplitude of the A0 wavelets differs from FD simulation. The FD simulation also simulates the A1 mode, this has not been taken into account in the FT simulation. In general the results of the FT simulation seem to agree with the results of the FD simulation.

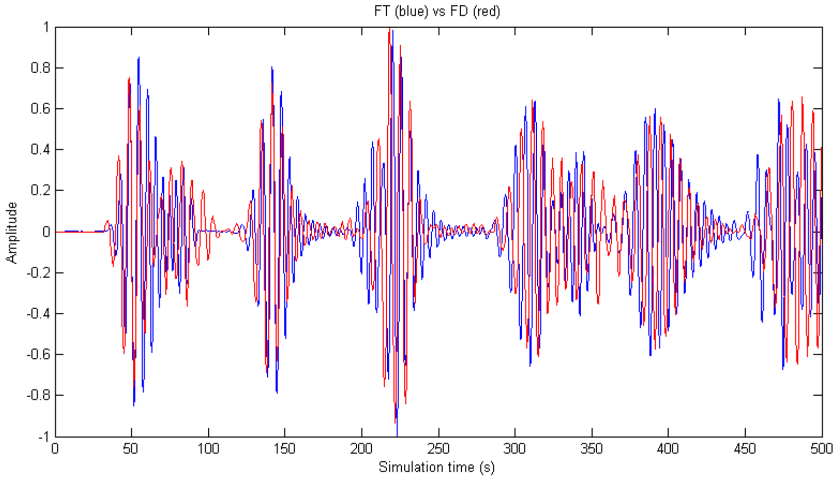

Figure 19: Comparison between the FT simulation (blue) and the FD simulation (red).

Another simulation was done to compare the FT simulation to measurements. In this simulation the shear velocity of the material has been set to 3220 m/s based on the properties of the measured pipe (Figure 20). The arrival time of the wavelets corresponds quite well. The FT simulation differs in amplitude from the measurement because of a small difference in wavelet slope. This is especially apparent in the later arrivals where dispersion stretches the frequencies apart. The amplitude of the measurement also tends to decrease in time because of geometric spreading, something that is not modelled in the simulation. For the inversion only the arrival time of the wavelets is important.

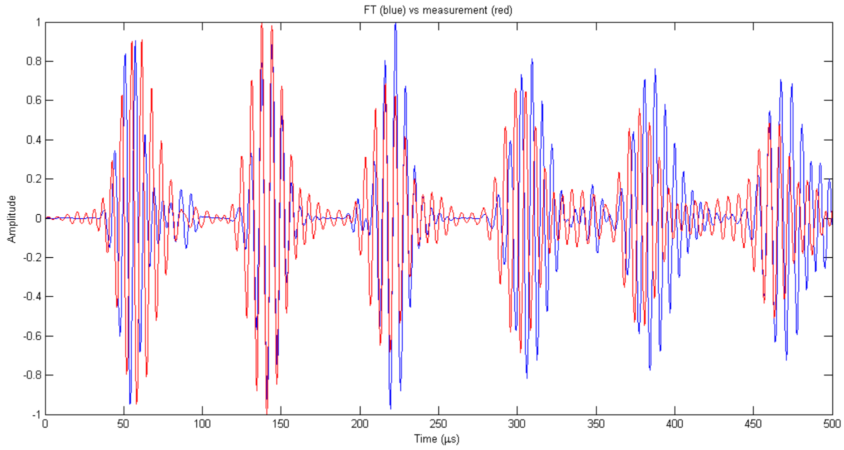

Figure 20: Comparison between the FT simulation (blue) and a measurement (red).

3.4 Window function

A Matlab function has been written to window the S0 mode from the experimental data. The script predicts the time of the S0 wave arrivals from the dispersion curves for the group velocity (Paragraph 3.1). First the radius and the source receiver distance is defined. Then using a constant wall thickness the time of arrival of the wavelets is calculated. At these positions the measured signal will be windowed using a flat top window with cosine flanks (Figure 21).

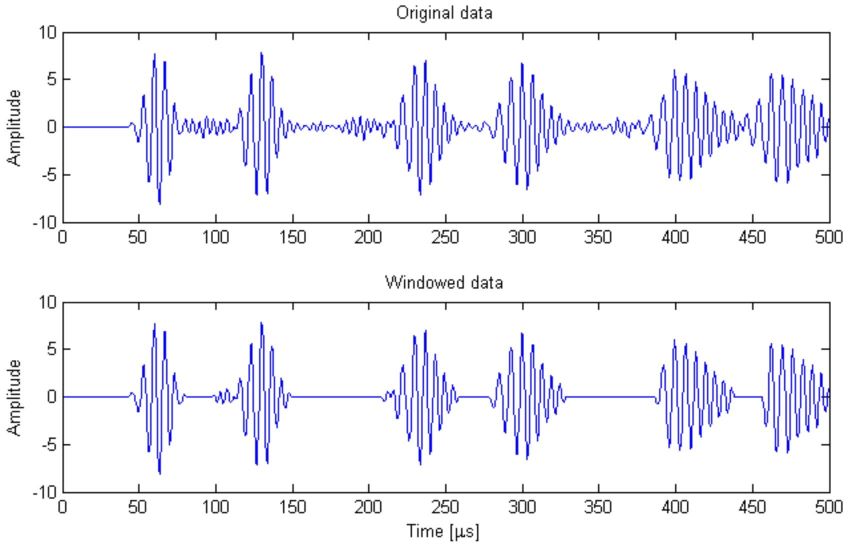

Figure 21: Simulated data from the FD simulation with a source receiver distance of 18 cm. On top without window and on the bottom with window.

4 Experimental measurements

Measurements have been performed on a test pipe in the TNO lab. The test pipe has artificially made defects to simulate corrosion spots. With the test pipe the reproducibility and SNR have been determined. Different wavelet characteristics have also been investigated.

4.1 Measurement setup

The measurement setup consists of: a pipe, two EMATs, a Ritec pulse generator, and a pc.

In the TNO lab there is a 6 m long pipe with an inner diameter of 10 inch (254 cm) (Figure 22). The pipe has a nominal wall thickness of 8 mm, at some areas the wall thickness has been artificially reduced. These areas represent wall thickness loss by corrosion and are observable from the outside of the pipe. On a piece of tape at a section of pipe the distances from the pipe end has been marked ranging from 160 cm to 250 cm. The marked section has sections with normal wall thickness as well as sections with an artificial defect. Most of the pipe is covered in mill scale. This is a brown layer that is created when the pipe was produced.

Figure 22: The pipe in the TNO lab. It is a 10 inch pipe with a nominal wall thickness of 8 mm.

Two EMATs were specially made, one EMAT is built as a transmitter the other as a detector. The EMATs are designed to mainly excite/receive the S0 mode. They each have four coil turns in meander configuration. The EMATs have a socket for the input or output signal. They are secured with screws on two beams that are joined with a hinge forming a single measuring unit. By loosening the screws the EMATs can be displaced along the length of each plate. Each EMAT has two pairs of wheels on the bottom so it can move along the length of the pipe (Figure 23). The EMATs are placed so that both sets of wheels touched the surface of the pipe. The distance between the centre of the source and receiver EMAT is 20.5 cm measured along the circumference of the pipe. The lift-off of the EMATs is 1.4 mm at the centre and 3.4 mm at the sides. The coil size is approximately 5.1 cm by 6.6 cm with the length being parallel to the circumference of the pipe.

Figure 23: Picture of the EMATs on the pipe.

A Ritec RPR-4000 pulse generator is used to produce the transmitted sine burst, it is connected with the source EMAT. The pulse generator is able to modify the characteristics of the input wavelet. This includes the centre frequency, number of cycles and amplitude. The pulse generator is also connected to the receiver EMAT. It also amplifies and filters the detected signal.

The digitiser inside the pc is connected to the pulse generator. It records the measured wavelet as well as the input wavelet. It uses a program to start and record the measurements. When a measurement is started a trigger signal is send to the pulse generator to generate a pulse. A signal is sent back to the pc to notify the program that it can start recording for a set time. After the measurement is done the program waits for some time to allow the wavelet to fade away before starting the next measurement. However, low frequencies take a long time to fade away so some remnants might exist in the next measurement. The time between each measurement has therefore a small variation so any wavelets from previous measurements can be averaged out.

4.2 Initial measurements and data processing

Some initial measurements were carried out on the pipe to get a cursory look at the measured signal. The goal was to develop a procedure to process the raw data and test the measurement setup.

The EMATs ware placed at a section of pipe with mill scale. The settings used for the pulse generator are: centre frequency of 150 kHz, 3 cycles, 70 dB gain and 3.85 V bias. The signals are recorded with a sampling interval of 300 ns and 2048 measurement points. The total measuring time is 614 µs. A source receiver distance of 20.5 cm has been used, this is an acceptable distance according to the results of the FD simulation.

In Figure 24a the raw measured signal is shown. At time 0 µs to 70 µs there is some high amplitude noise. This is caused by crosstalk between the receiver input and transmitter output on the pulse generator. The crosstalk covers the first S0 arrival. This is not a problem because as stated earlier, the first arrival does not contain information about the entire circumference. The other S0 arrivals have higher amplitude than the noise. A0 modes cannot be identified. Figure 24b shows the signal after it is averaged from 500 measurements. This reduces the noise. It now becomes apparent that there is an A0 wavelet between 330 µs and 370 µs. Finally in Figure 24c the crosstalk has been suppressed by using a window over the rest of the signal. The signal has also been frequency filtered. A band pass filter has been applied around the centre frequency. The settings for the filter are: 100% amplitude for frequencies between 20 kHz under the centre frequency and 20 kHz above centre frequency, 0 % amplitude for frequencies lower than 40 kHz under the centre frequency and higher than 40 kHz above centre frequency. A Matlab script has been written to process the measurements in the above described way. The measurements shown in this thesis are all processed this way unless otherwise mentioned.

a.

b.

c.

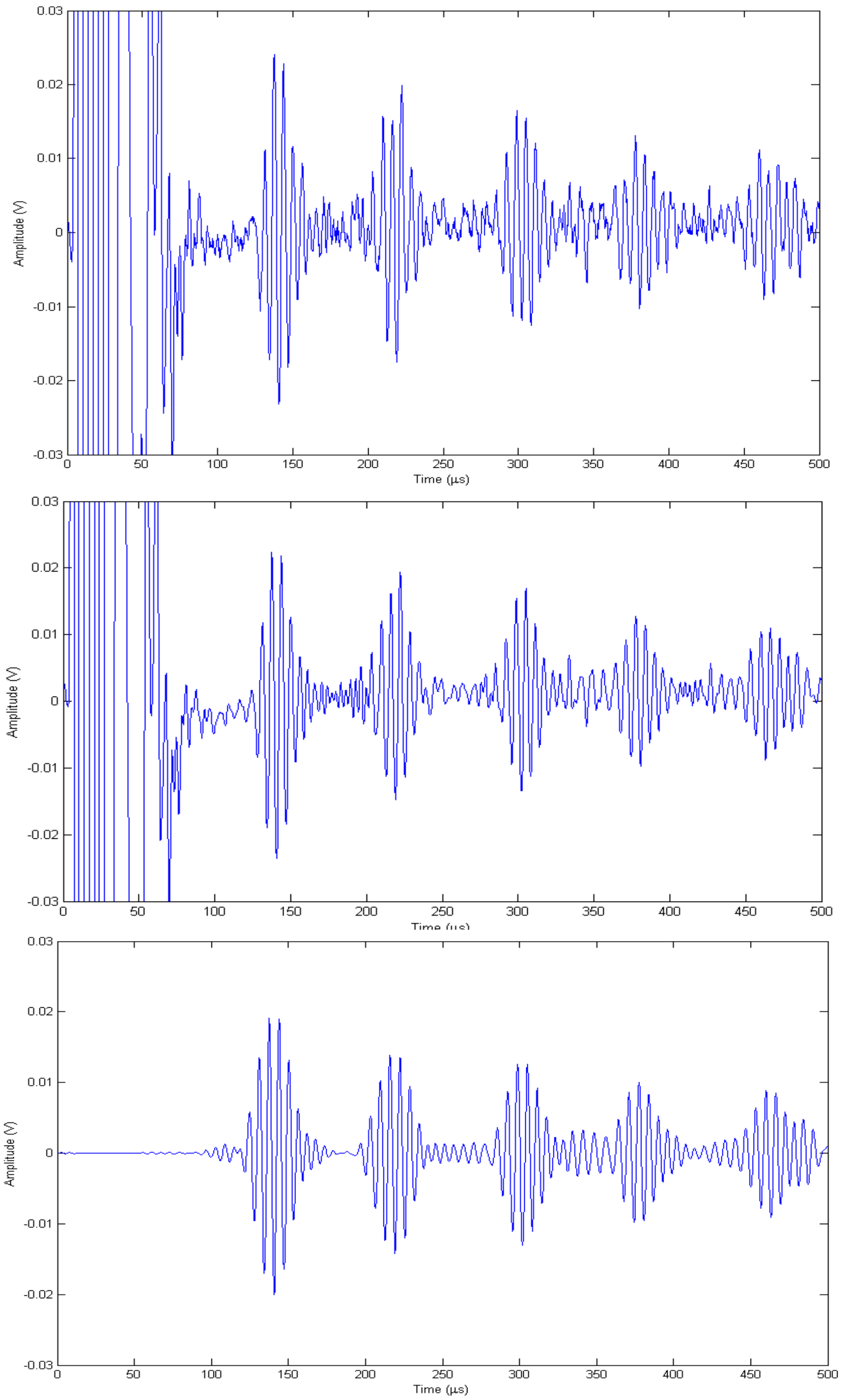

Figure 24: (a.) raw measured signal, (b.) signal averaged from 500 measurements, (c.) windowed and frequency filtered signal.

4.3 SNR and reproducibility measurements

It is important for the measurements that the results are reproducible. This is directly affected by the Signal to Noise Ratio (SNR) of the measurements. The noise of the measurement setup has three primary sources: electrical crosstalk, thermal noise and magnetostriction caused by mill scale. Because of the predictable location of the crosstalk within the measured signal it can be separated from the rest by the use of a window to exclude the crosstalk. Thermal noise cannot be reduced effectively except by averaging the signal.

It is expected that the mill scale would degrade the reproducibility of the measurement because of unwanted magnetostriction inside the scale layer. Measurements have been done to measure the SNR and reproducibility at sections of the pipe with mill scale and without mill scale. In practice mill scale is not a problem because it is not present on pipes used in the industry.

By calculating the SNR as function of the number of means of the noise, it can be decided how often the measurement signal should be averaged to have a good SNR. This has been done by first measuring the noise signal of the receiver without a source signal 1000 times. The noise is then cumulative averaged: the first noise signal stays the same, the second is summed with the first and divided by two, the third is summed with the first and second noise signal and divided by three, etc.. The maximum amplitude of the noise is then divided by the maximum amplitude of a normal measurement signal to obtain the SNR. This has been done for a position along the pipe with and without mill scale. A measurement has also been done with a plastic sheet that acts as an insulator between the EMAT and the pipe wall.

The reproducibility of the measurements has been investigated by comparing the difference between measurements on the same position. On six positions of the pipe five measurements have been done while moving the EMAT to another position between each measurement. Another five measurements have been done while the EMAT was not moved. This has been done once on a section with mill scale and once on a section without mill scale. In total 14 measurement sets of five measurements each has been done.

4.3.1 SNR results

The measurement signal of two sections, one with and one without mill scale is compared in Figure 25. The arrival times of the wavelets are not shifted. It is also seen that the amplitude of the signal without mill scale is lower. The amplitude of the A0 mode is especially lower in the signal measured on the section without mill scale. Notice that the amplitude of the second S0 arrival is lower than the first arrival unlike the measurement done on mill scale. This is because the A0 mode that overlaps the second S0 arrival is weaker. It is clear that magnetostriction inside the mill scale layer has an effect on the signal.

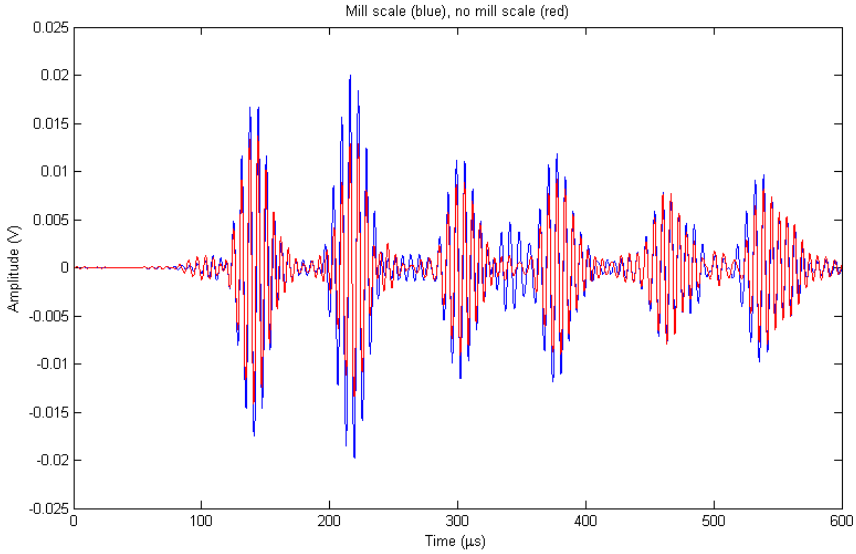

Figure 25: Comparison of a measurement done on a section with mill scale (blue) and a section without (red).

The SNR as function of the number of means is plotted in Figure 26. The SNR as function of number of means for the measurements with mill scale seems linear. For the measurements without mill scale however the SNR curve has a lower gradient and seems to flatten out at the end. The SNR without mill scale seems lower because the maximum amplitude of the measured signal is lower. This however, is only due to the reduction in amplitude of the A0 mode inside the second S0 arrival. Based on this result the procedure to average the measurement signal 500 times is sufficient to reach an SNR of 70 dB. The SNR is sufficient when compared to the 35 dB minimal SNR requirement of similar measurement methods using ultrasound by TNO.

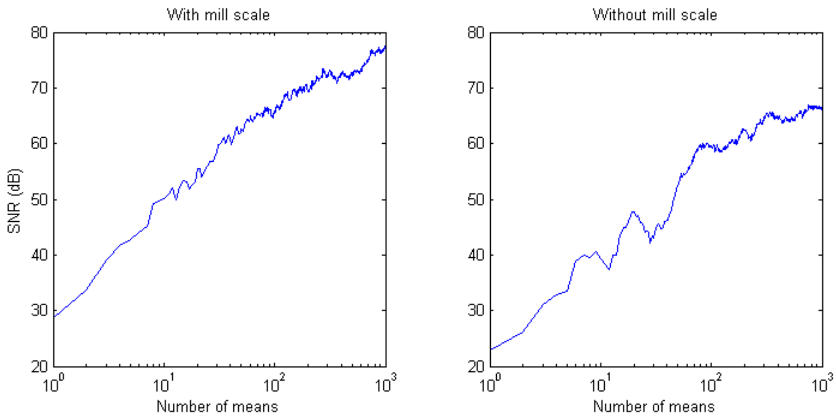

Figure 26: Comparing the SNR as function of number of means between with and without mill scale sections of the pipe. The maximum number of means is 1000.

In Figure 27 the SNR is compared when measuring with and without a plastic insulator. It seems that the plastic insulation has no significant effect on the SNR. The use of the plastic insulator was omitted during further measurements. Note that this measurement was done when not all of the EMATs wheels touched the pipe wall. The lift off was therefore higher and signal amplitude was lower than the previous measurement.

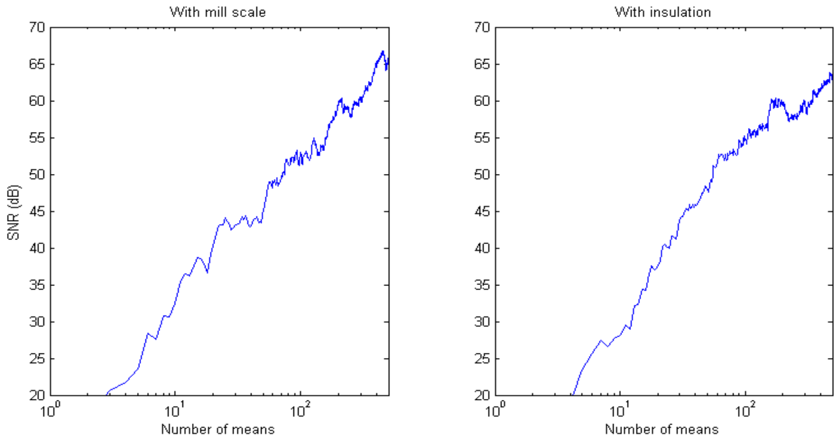

Figure 27: Comparing the SNR as function of number of means between with and plastic insulator between the EMAT and pipe. The maximum number of means is 500.

4.3.2 Reproducibility measurements results

In Figure 28 the signals measured when moved between each measurement are plotted. 30 measurements in total are plotted in the same figure each with a different colour. This is also done for the measurements with and without mill scale. The same has been done for the five measurements without moving between the measurements in Figure 29. By comparing these two figures it can be seen that by moving the EMAT the signal is less reproducible. It can also be seen that mill scale does not appear to affect the reproducibility.

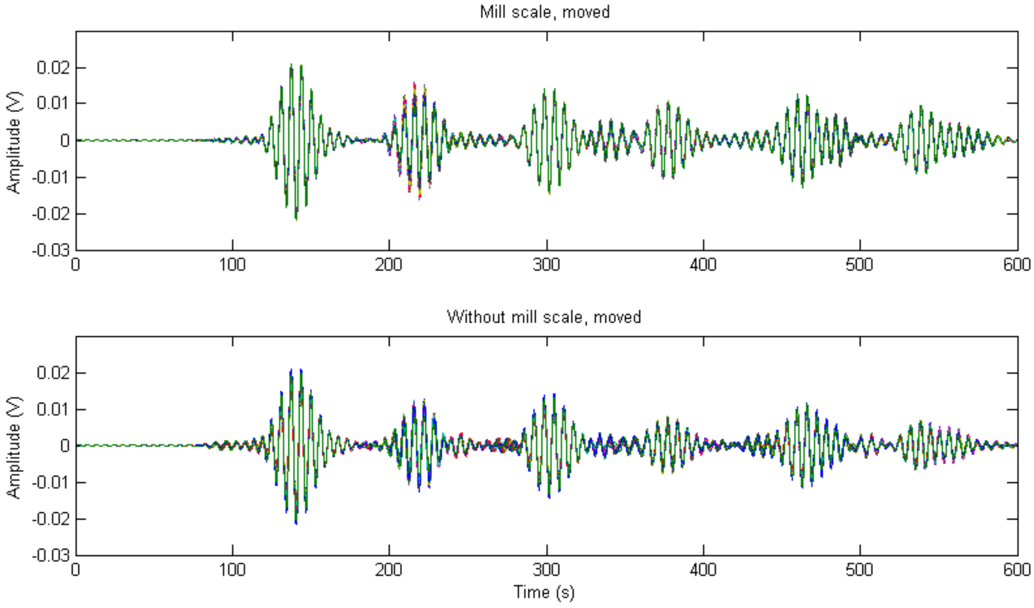

Figure 28: 30 measurements measured while moving after each measurement plotted in the same figure. Top with mill scale, bottom without mill scale.

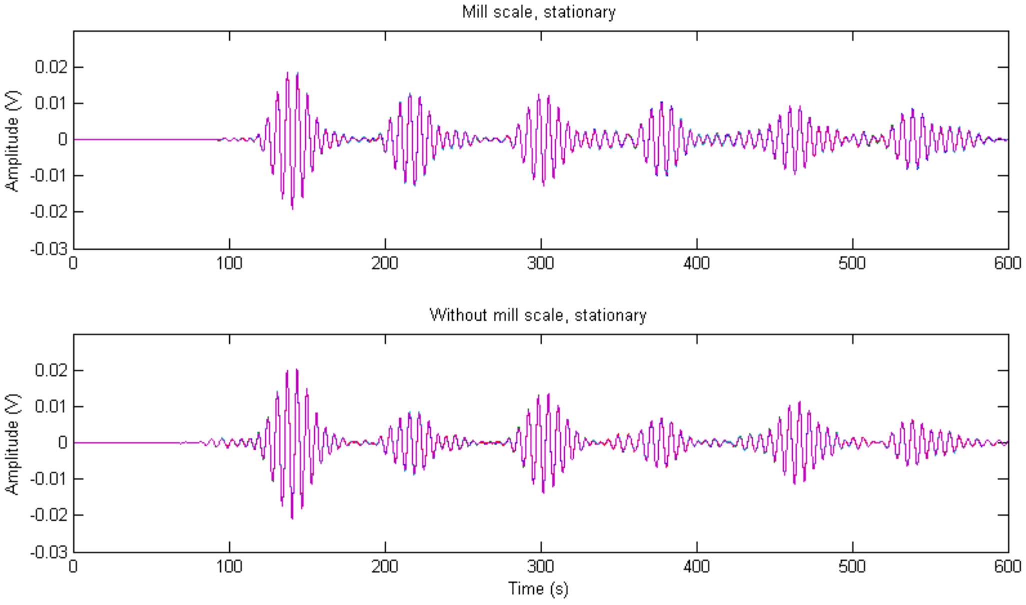

Figure 29: 5 measurements measured without moving between the measurements plotted in the same figure. Top with mill scale, bottom without mill scale.

The difference between the signals has been quantified by taking the difference between the first wave measured at each position and each of the other waves measured at the same position (Figure 30). In the first plot of the figure the five signals measured at one position is plotted together. The four plots below are the difference between the first signal and the others.

The absolute value of the resulting difference waves is summed along the time axis. This yields a value for the surface under the difference wave, it has been called the 'total difference'. The total difference has been used as a measure of how well the signals match. However, in fact there are two potential differences between waves: phase and amplitude. Knowing the difference in phase is the most important because the wall thickness measurement relies on phase differences. The total difference covers both of them.

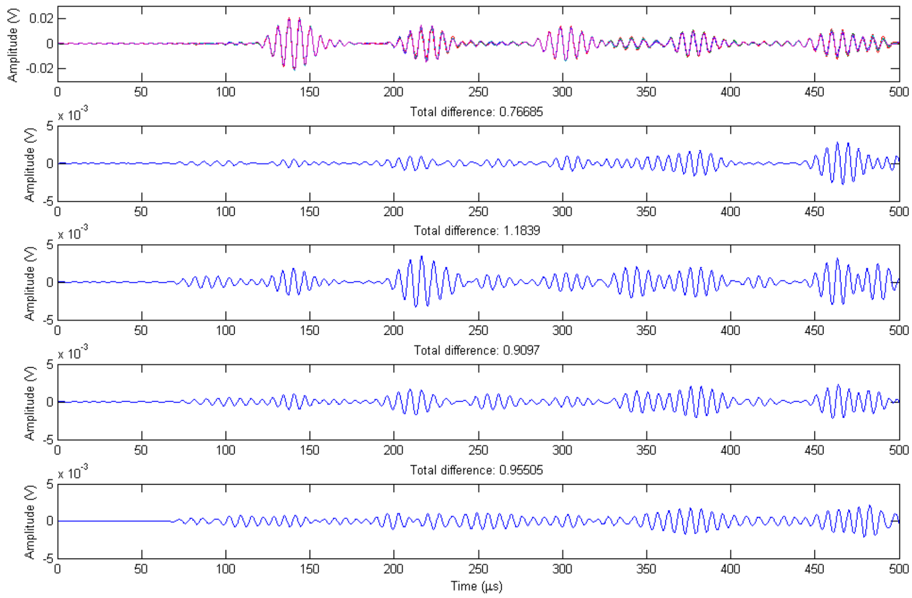

Figure 30: The difference between the first signal and the other four at the first position is shown. On the first plot the five signals are plotted together.

The total difference has been calculated for the measurements at each position (Figure 31). Each group of four measurements represents the total difference between the first and the other measurements done at the same position. The different types of measurements are indicated in the figure. From bar plot can be seen that the total difference without moving the EMATs is lower. The spread between the total differences is also larger when the EMAT is moved. The total difference of the stationary measurements with and without mill scale is similar. It can therefore be concluded that moving the EMATs is the largest detriment to the reproducibility and that mill scale does not have an influence on the reproducibility. Something to note is that the total difference increases in most of the moved measurement sets. This may be caused by increasingly inaccurate positioning of the EMAT at the same position after each measurement. Minor irregularities of the wall thickness along the length of the pipe might cause the difference in measurement signals.

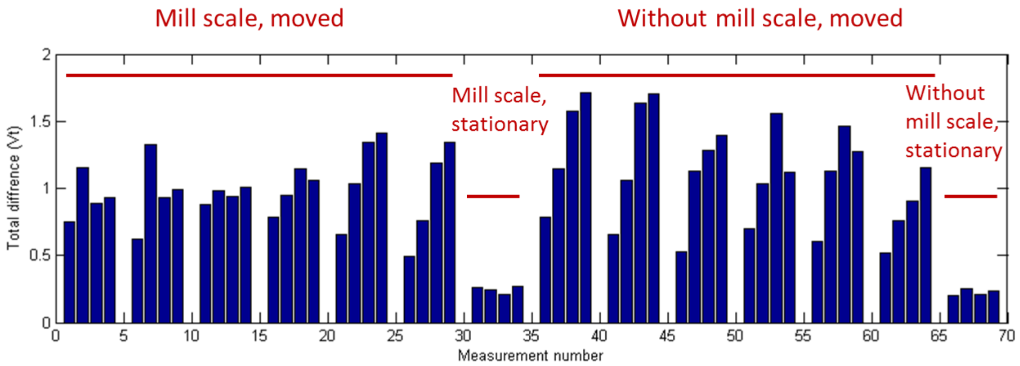

Figure 31: Bar plot of the total difference calculated for each of the measurement sets. The measurements between 30 to 35 and 65 to 70 are the measurements done without moving. The measurements left of the 35 mark are done with mill scale, the measurements on the right is done without mill scale.

4.4 Different source wavelets measurement

In the simulations a centre frequency of 150 kHz and a cycle number of three has been used. Measurements have been done with different values for the centre frequency of the excited wave to investigate the optimal excitation frequency of the EMAT. The number of wave cycles that define the length of the wavelet has also been varied. Frequencies between 100 kHz and 250 kHz and cycles of one to five have been studied. The measurements were done on the same spot with mill scale. When the frequency was varied the number of cycles used was three, when the cycles were varied the centre frequency used was 200 kHz. The pulse generator settings remain the same as the SNR measurement except for the sampling interval which was reduced to 250 ns to accommodate the higher frequencies. The total measuring time is 512 µs.

4.4.1 Different source wavelets measurement results

Only a few measurements will be discussed, the results of the others are found in Appendix C. In Figure 32 three measurements are shown, each signal has a different number of cycles excited in the source wavelet. As can be seen from the figure the amplitude gets higher if the amount of cycles increases. The length of the wavelet also increases. Because using a different number of cycles does not bring any advantage, it has been decided to remain using three number of cycles.

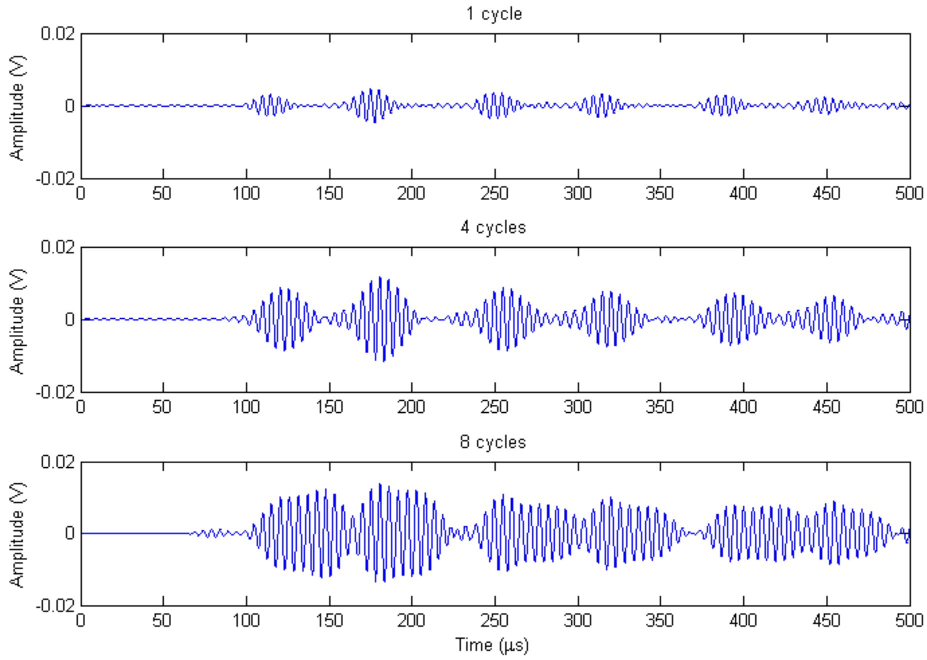

Figure 32: Signals with a centre frequency of 200 kHz with different number of cycles. 1 cycle (top), 4 cycles (middle) and 8 cycles (bottom).

Different frequencies are compared in Figure 33. Higher frequencies cause the amplitude of the wavelet to increases. The A0 mode amplitude relative to the S0 seemed to change as well, this will be discussed further in the next section. The wavelets also become more dispersive, this is to be expected when looking at the dispersion curve . This is in accordance with the dispersion curves (Figure 11), the slope on the dispersion curve increases at higher frequencies. Thus for higher frequencies the sensitivity to defects increases but a having too much dispersion can cause the wavelets to overlap.

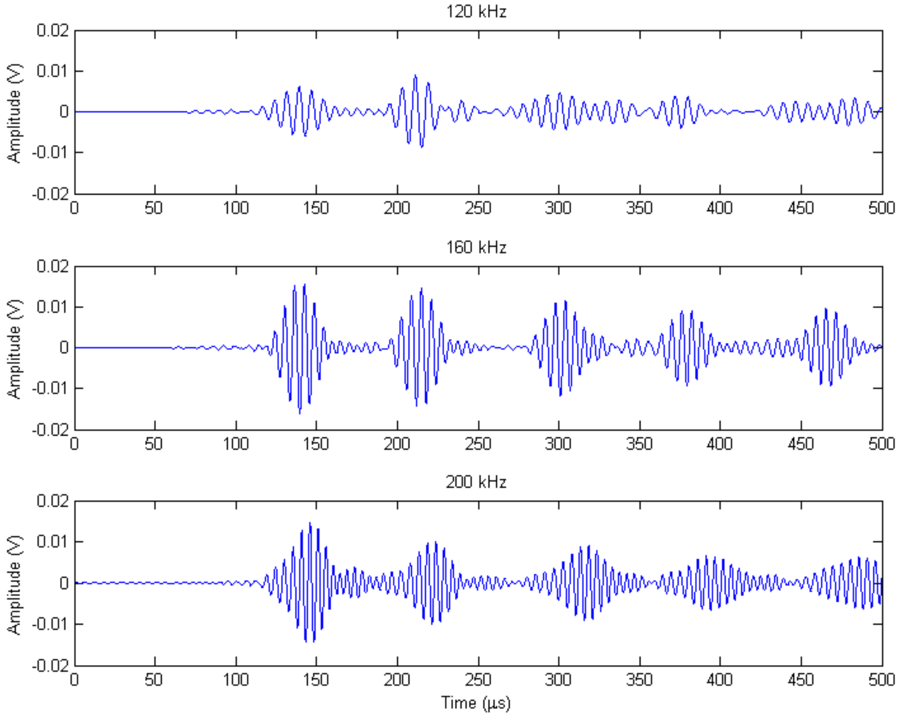

Figure 33: Signals with three cycles with different centre frequencies. 120 kHz (top), 160 kHz (middle) and 200 kHz (bottom).

In Figure 34 the measurements with frequencies of 150 kHz and 180 kHz are compared. It can be noted that the amplitudes of the A0 mode is lower for the 180 kHz measurement. In Figure 35 the frequency spectra of an S0 and A0 wavelet is plotted for both frequencies. This is done by windowing a single wavelet from the unfiltered signal and Fourier transforming it. The relative amplitude difference between the S0 and A0 mode is higher at 180 kHz centre frequency. Therefore it has been chosen to use a centre frequency of 180 kHz for future measurements and to remain using three cycles. The digital frequency filter used for data processing is relatively narrow banded to take advantage of the slight dip in the A0 spectrum near 180 kHz.

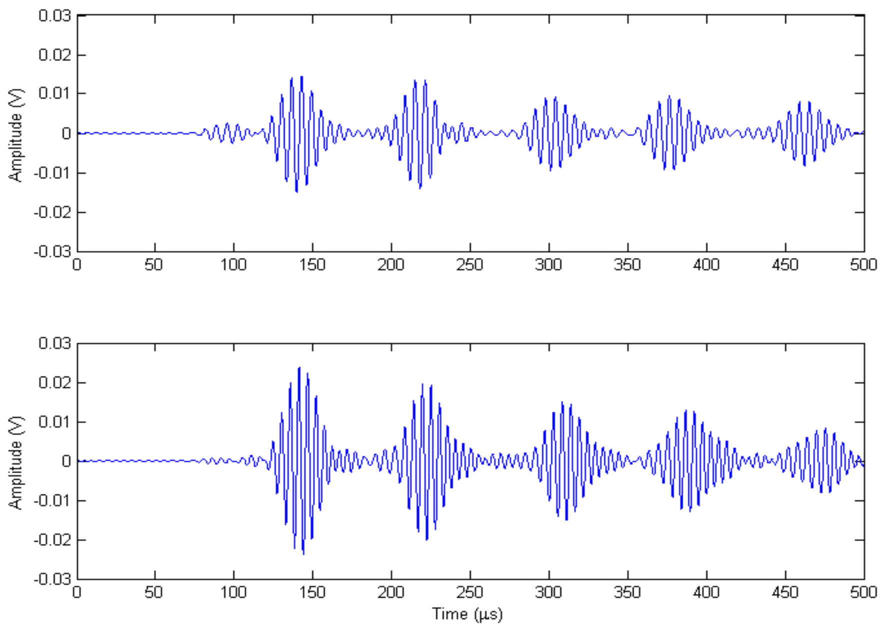

Figure 34: Comparison of signals with 150 kHz (top) and 180 kHz (bottom).

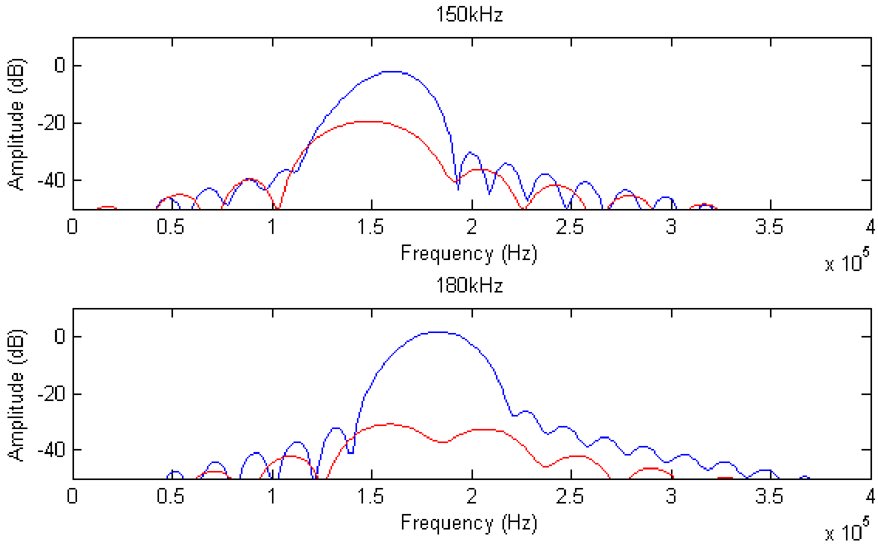

Figure 35: Comparison of the frequency spectrum of an S (blue) and an A (red) wavelet, 150 kHz (top) and 180 kHz (bottom).

5 Defect measurement on pipes

A measurement series has been done along a section of the length of three pipes. The first pipe is a pipe in the TNO lab with artificial defects. All previous measurements have been done on this pipe. The second pipe is a section of a pipeline from Shell, a multinational oil and gas company. It has an inner diameter of 10 inch just as the TNO pipe but with real corrosion spots. The final pipe, located in the same building, is a section of pipeline of the Dow Chemical Company. It is an 8 inch pipe with real corrosion, see Appendix D for a table with the start pipe sizes.

5.1 Measurement approach

The measurement setup consists of a tape measure that has been fitted on a section of the length of the pipe. The EMAT measuring unit is outfitted with a laser pointer that is secured to the measuring unit with a clamp. The laser points at the tape measure so displacing the EMATs can be done accurately (Figure 36). The settings for the pulse generator remained the same except for the centre frequency. It was changed to 180 kHz. A measurement has been done in steps of one cm along the marked section.

The measured data is processed in a similar manner as described earlier. The only difference is that the signal is corrected for dispersion effects. The time of the maximum amplitude of the first arrival has been calculated for each signal with a Matlab script. The difference in the arrival time is a measure for the wall thickness loss.

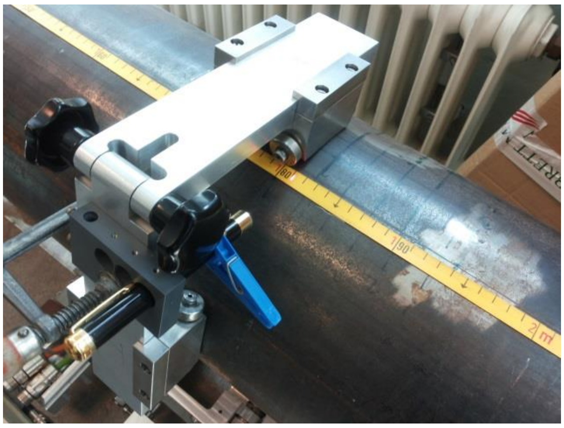

Figure 36: A picture of the measurement unit with a laser pointer on the TNO pipe.

5.2 TNO pipe

The pipe in the TNO lab has four sections with defects. Two of them are small in size and deep while the others have a large surface are and are shallow (Table 1, Figure 37). There are also three sections without mill scale (Table 2, Figure 38). Note that positions of these locations have a small offset in the measurements because of the distance between the laser pointer and middle of the EMAT coils. A section of 370 cm has been measured starting 126 cm from the left edge of the pipe.

Table 1: Locations of the artificial defects on the TNO pipe. The width is the size of the defect measured along the circumference of the pipe. The defects have an oval shape, the depth given is the maximum depth.

Defect	Position (cm)	Width (cm)	Depth (mm)
A	59-69 ± 0,5	7,2 ± 0,5	5.1 ± 1
B	110-150 ± 2	20 ± 2	1.5 ± 2
C	177-187 ± 0,5	5,6 ± 0,5	5.1 ± 1
D	250-315 ± 2	23 ± 2	1.7 ± 2

Table 2: Sections of the TNO pipe without mill scale.

Section	Sections without mill scale (cm) ± 2 cm
E	79-119
F	277-287
G	300-325

Figure 37: This picture shows the defect spot of one of the large defect spots (left) and small defect spots (right) on the TNO pipe.

Figure 38: Picture of a section without mill scale.

An image has been made from all the measured signals as function of the measured length along the pipe (Figure 39). In Figure 40 the same image is shown but with the defect spots and sections without mill scale marked. An approximation of the shape of wall thickness profile has been made by plotting the arrival times of the first wavelet as function of the measured length (Figure 41). The highest arrival time has been subtracted from the data for easier comparison. A moving average of three samples has been used to smooth the plot for display purposes. The defects might be deeper than shown.

It can be noted that the relative depth of the defects are not represented correctly in the wall thickness profile approximation. This is because this approximation assumes that the defects all have the same shape. However, this is not the case as for example: the deep defects have a much higher depth gradient than the shallow ones. It is also worth noting that the absence of mill scale does not seem to have an impact on the measurements except for the last defect spot. The lack of mill scale seems to artificially increase the wall thickness at that location.

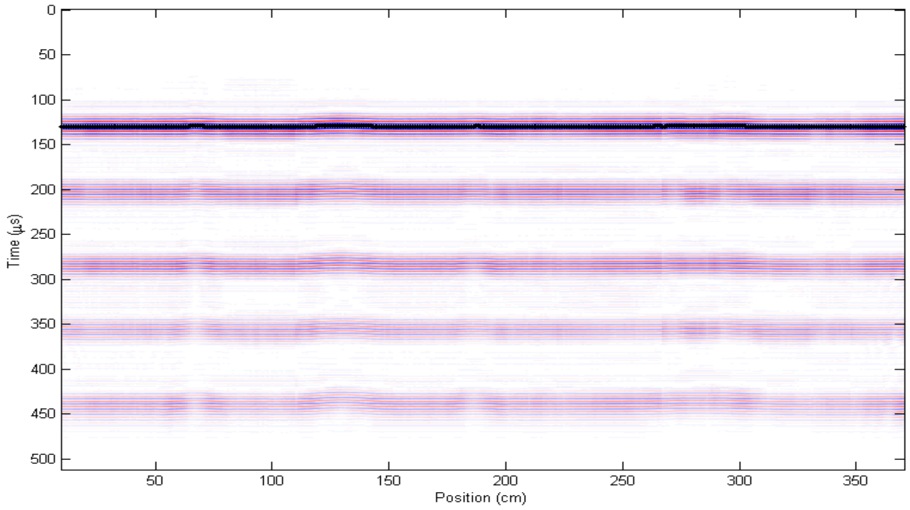

Figure 39: Image of all the measurements taken across the length of the measured section of the TNO pipe. The maximum amplitude of the first wavelet is indicated in black.

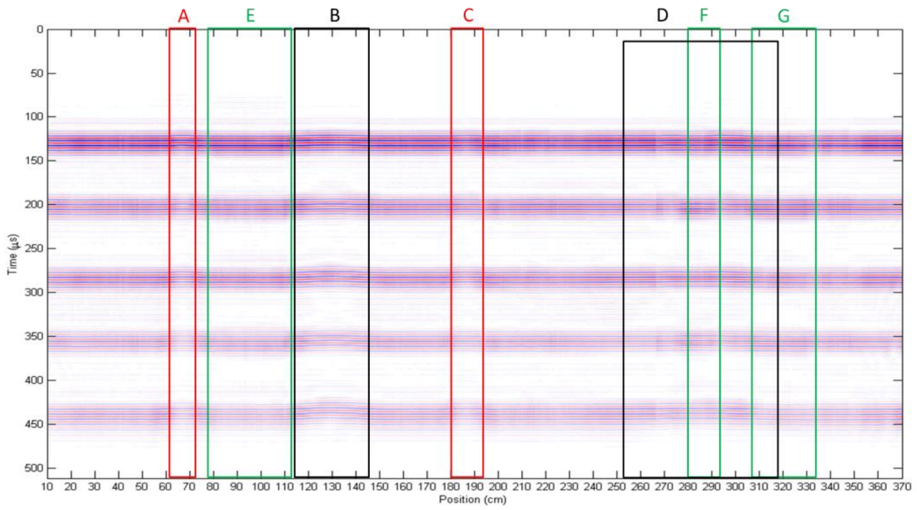

Figure 40: The same image as in Figure 39 but with defect spots and sections without mill scale outlined. A and C are the deep and small defects. B and D are the shallow and wide defects. E, F and G are the sections without mill scale (Table 1 and Table 2).

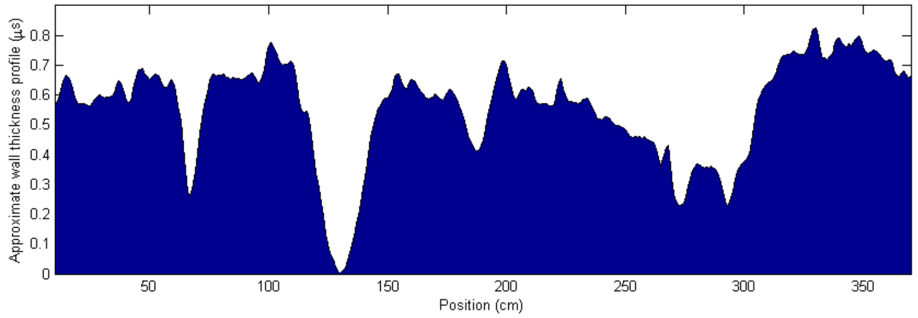

Figure 41: An approximation of the shape of the wall thickness profile of the TNO pipe. A floating average of three samples has been used.

5.3 Shell pipe

The Shell pipe has real corrosion spots (Figure 42). The inside of the pipe has corrosion running across the length of the pipe. This type of corrosions is called bottom of the line corrosion. This is a typical form of corrosion in crude oil pipelines. The oil contains a small amount of salt water which collects at the bottom of the pipe.

A large corrosion spot is present at one location at the bottom of the pipe (Figure 43). This corrosion spot is covered by a welded support that is located at 161 cm to 200 cm. A section of 300 cm has been measured. The measurements are compared to a different measurement of the pipe wall made using ultrasound tomography. In Figure 44 a 2D image of the wall thickness of the pipe is pictured. This image is made using conventional ultrasound techniques. The corrosion along the bottom can be clearly seen. The white box is the area where the welded support is located, no measurements were done there because of inaccessibility.

Figure 42: Picture of the Shell pipe with EMATs.

Figure 43: The welded support at the bottom of the Shell pipe. Corrosion is visible from the outside of the pipe.

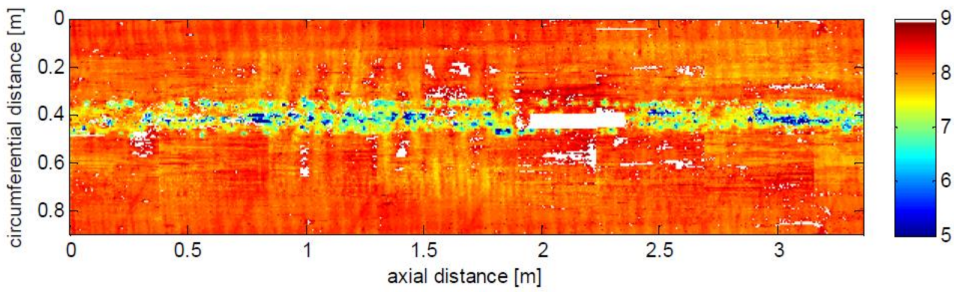

Figure 44: A 2D image of the wall thickness of the pipe. The colour represents the wall thickness. The white box is the position of the welded support. This image is from a different measurement using conventional ultrasonic techniques [10]

In Figure 45 the image of the measurements as function of measured length is shown. The approximate wall thickness profile shape is compared in Figure 46. The general shape seems to correspond to the wall thickness profile acquired from tomography.

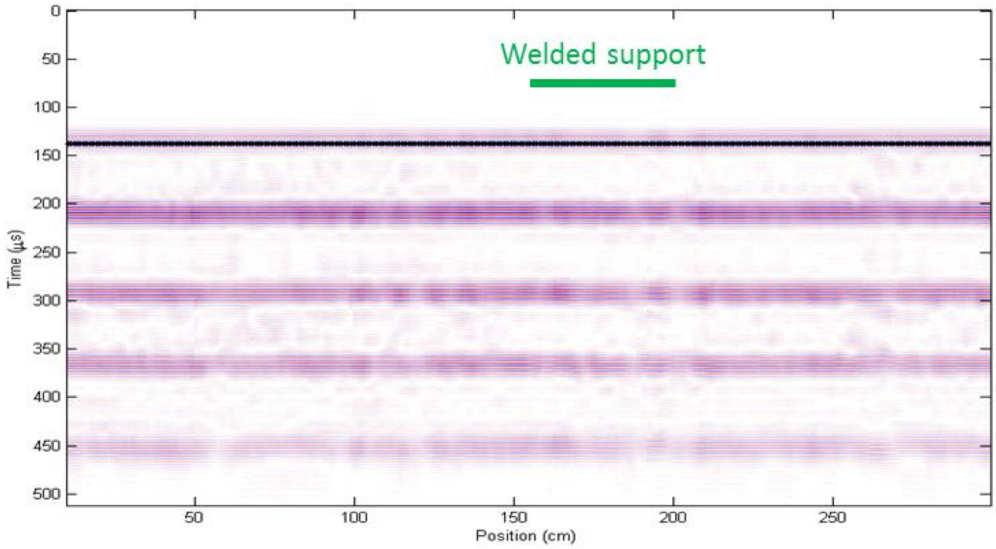

Figure 45: Image of all the measurements taken across the length of the measured section of the Shell pipe. The location of the welded support and maximum amplitude of the first wavelet is indicated.

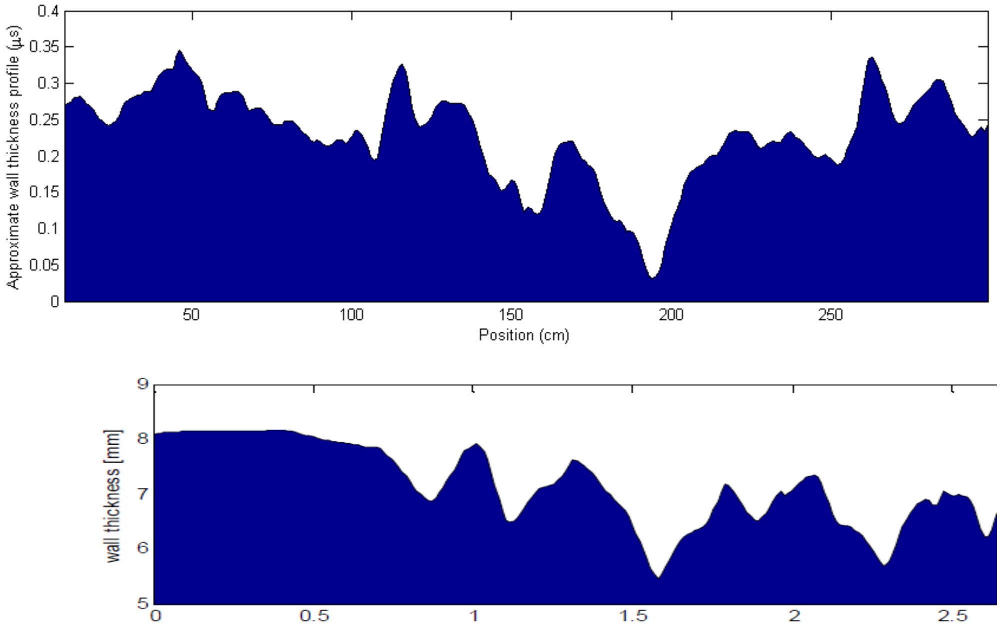

Figure 46: An approximation of the shape of the wall thickness profile of the Shell pipe (top). A floating average of nine samples has been used. The results are compared to the wall thicnkess profile of the pipe made by another measurement using ultrasound tomography (bottom).[10]

5.4 Dow pipe

A section of 180 cm has been measured on the Dow pipe. The Dow pipe is an 8 inch pipe, the source receiver distance was therefore changed to 16.4 cm. The wheels of the EMATs are not big enough to not let the EMATs touch the pipe. Therefore the wheels have been wrapped in tape to increase the lift off. The Dow pipe has an area with pitting corrosion located at 75 cm to 104 cm (Figure 47, Figure 48). Pitting corrosion is a form of corrosion that is concentrated in a small area. On either side of this location are sections where there used to be piezoelectric transducers used in other measurements (Figure 49). The coating is removed on these locations (10 cm to 19 cm and 160 cm to 174 cm).

Figure 47: The area with corrosion on the Dow pipe.

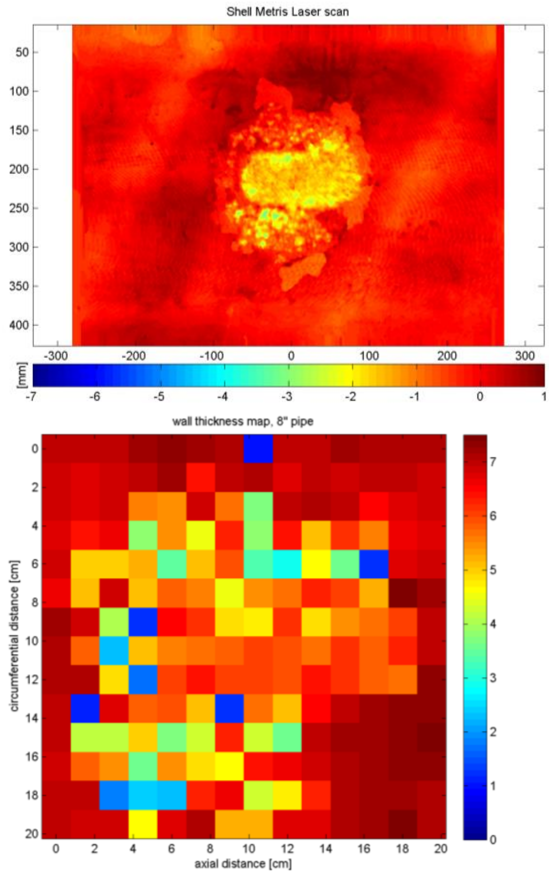

Figure 48: A laser scan covering the area with pitting corrosion (top). It underestimates the depth of the defect. A close up image produced from an ultrasonic measurement gives a better view of the pitting (bottom). This has been done in previous measurements by TNO.

Figure 49: One of the locations with removed coating. Piezoelectric transducers used to be attached here.

The measurements along the measured length are shown in Figure 50. In the approximation of the shape of the wall thickness profile the corrosion spot in the middle can be seen (Figure 51). The locations with removed coating are also visible on in the figure. This indicates that coating affects the measured signal.

At the left half of the location of the expected corrosion an increase of the wall thickness is detected. This might be caused by the coating. The top image of Figure 48 also indicates an area around the corrosion spot with higher wall thickness. The right half of the corrosion spot in the measurements has as expected a lower wall thickness. It does however seem to underestimate the depth of the pitting. This is probably caused by the small size of the pitting, the step size might be too high or the width of the EMAT is too long to accurately detect them.

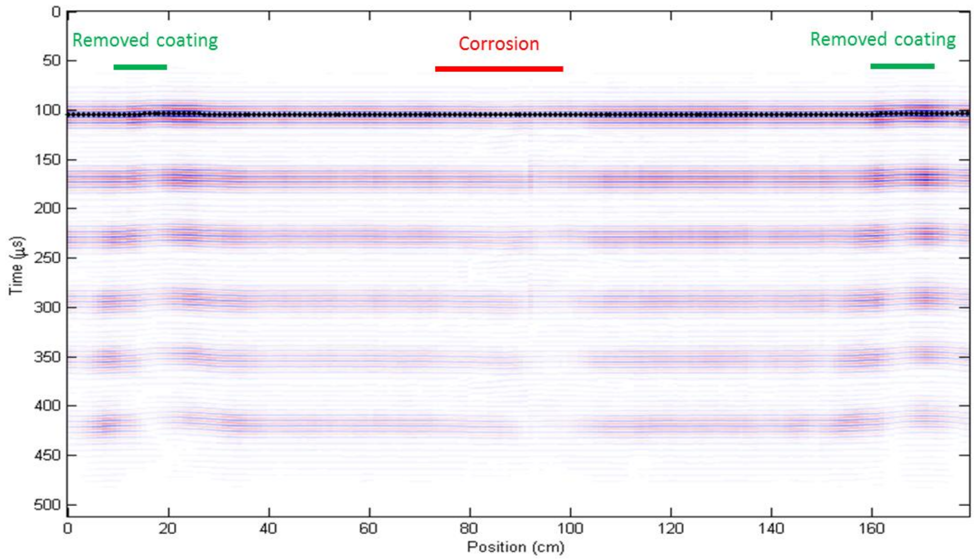

Figure 50: Image of all the measurements taken across the length of the measured section of the Dow pipe. The position of the maximum amplitude is indicated in black.

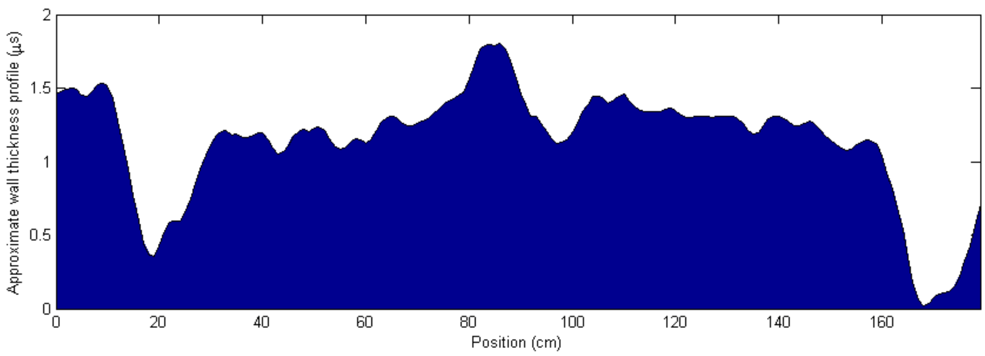

Figure 51: An approximation of the shape of the wall thickness profile of the Dow pipe. A floating average of three samples has been used**.** Note the difference in y axis scale from the previous wall thickness approximations.

6 Conclusion

The goal was to evaluate if defect sizing in pipelines was possible using Lamb waves and EMATs. This research shows that it is indeed possible. Although a quantitative wall thickness profile has not been made, it is a relatively small step to make a complete wall thickness profile from the results.

A semi analytical simulation for Lamb waves in the pipe circumference has been made with Matlab. The results of this simulation correspond to results of the finite difference simulation and experimental measurements.

From the results of the SNR and reproducibility measurements can be concluded that the measurements have a SNR of 70 dB when taking 500 means of the measured signal. The goal was to have a minimum of 35 dB SNR. The reproducibility of the measurements is also sufficient. The largest cause of differences between measured signals at the same position is caused by displacing the EMATs. Sections of a pipe with mill scale seem to have no impact on the reproducibility. However sections without mill scale seem to excite A0 wavelets with lower amplitude, thus improving the signal by lowering the unwanted A0 mode.

Measurements conducted with other centre frequencies and different numbers of cycles have resulted in the use of a 180 kHz centre frequency instead of 150 kHz used in the FD simulation. The reason was that the A0 mode featured lower amplitudes for the 180 kHz signal. The number of cycles used for the measurement has not changed from the value used in the FD simulation and remained at three cycles

A section along the length of three different pipes has been measured. One pipe in the TNO lab has artificial defects while the Shell pipe and Dow pipe had real corrosion spots. An approximation of the shape of the wall thickness profile has been made by comparing the time difference of the arrival of a wavelet in the measured signals. The defect areas of the approximated profile of the TNO pipe can be identified and related to known defect locations. The approximated wall thickness profile of the Shell pipe was compared to a wall thickness profile acquired by ultrasound tomography. The general shape corresponded. The measurements on the Dow pipe revealed that pipe coating affects the wall thickness profile. The approximation of the wall thickness profile underestimates the depth of the pitting corrosion. This is probably due to the small size of the pitting.

These measurements show that a loss in wall thickness can be identified. No wall thickness profile has been made but an approximation of the relative thickness of the pipe wall has been acquired.

For the actual thickness of the pipe wall the script of the FT simulation could be modified to fit the measured data to a defect spot. Then the wall thickness profile from the measurements could be compared more accurately to known pipe defects. Also to better quantify the defect the measurements could be done with the EMATs placed parallel to the length of the pipe, in other words rotating it by 90°. This should yield more precise information on the length of the defect. This can be combined with the other measurement to form a 2D estimation of the defect that should be more accurate.

7 References

[1] Lowe, M., Alleyne, D., & Cawley, P. (1998). Defect detection in pipes using guided waves. London: Elsevier.

[2] Rose, J. L. (1999). *Ultrasonic Waves in Solid Media.* Cambridge: Cambridge Univerity Press.

[3] Su, Z., & Ye, L. (2009). *Identification of damage using lamb waves.* Berlin: Springer.

[4] NDT Rescource Center. (2015, February 23). *Modes of Sound Wave Propagation*. Retrieved February 23, 2015, from NDT Rescource Center: https://www.nde-ed.org/EducationResources/CommunityCollege/Ultrasonics/Physics/modepropagation.htm

[5] The Pennsylvania State University. (2015, February 23). *Phase, Group, and Signal Velocity*. Retrieved February 23, 2015, from The Pennsylvania State University: http://www.personal.psu.edu/pjm11/groupandphasevelocityetc.htm

[6] Hübschen , G., & Diederichs , R. (2015, April 30). *Generation of Horizontally Polarized Shear Waves with EMAT Transducers*. Retrieved from ndt: http://www.ndt.net/article/0398/huebsch/hueb.htm

[7] Enthoven, D. (2014). *EMAT Design.* Delft: TNO.

[8] Van der Burg, W. (2014). *1-D Profiling using highly dispersive guided waves.* Delft: TNO.

[9] Cheng, Y., Deng, Y., Cao, J., Xiong, X., Ba, L., & Li, Z. (2013). *Multi-Wave and Hybrid Imaging Techniques: A New Direction for Nondestructive Testing and Structural Health Monitoring.* Basel: MDPI.

[10] Vos, H., & Volker, A. (2011). TNO-RPT-DTS-20011-01340: *Joint Industry Project - Ultrasonic Corrosion Monitor.* Delft: TNO.

[11] Puget Sound Pipe & Supply. (2015, June 3). *http://www.pspipe.com/*. Opgehaald van Metric Pipe Chart: www.pspipe.com/file_viewer.php?id=189

8 Appendix A: Assignment description

Corrosion and cracking are the two major issues regarding the integrity of industrial assets. Currently inspections are conducted at regular intervals to ensure a sufficient integrity level of these assets. Cost reduction while maintaining a high level of reliability and safety of installations is a major challenge. There are many situations where the actual defect location is not accessible, e.g., a pipe support or a partially buried pipe. In that case guided ultrasonic waves are used to detect and size defects. TNO is currently developing a method that uses guided waves that travel in the circumferential direction of a pipe to reconstruct the wall profile of corrosion.
The objective of the project is to evaluate a newly developed EMAT sensor on pipe with artificial and real defects. Special attention will be paid to the signal to noise ratio and the presence of other, not desired guided wave modes.
Moreover we will evaluate whether pitting can be detected as well. Numerical simulations will be used to improve our understanding about the interaction of guided waves with pitting defects.

9 Appendix B: About the company

TNO is a research organization with about 3000 employees. TNO focuses its research on industry, healthy living, defense and security, urbanization and energy. The goal is to bring people and knowledge together to create innovations that improves the industry and society in a durable way. The thesis research will be done in the PID department in the TNO establishment on the Stieltjesweg in Delft. The primary focus of the department is to develop measuring techniques using acoustic methods.

10 Appendix C: Different source wavelets measurement extended results

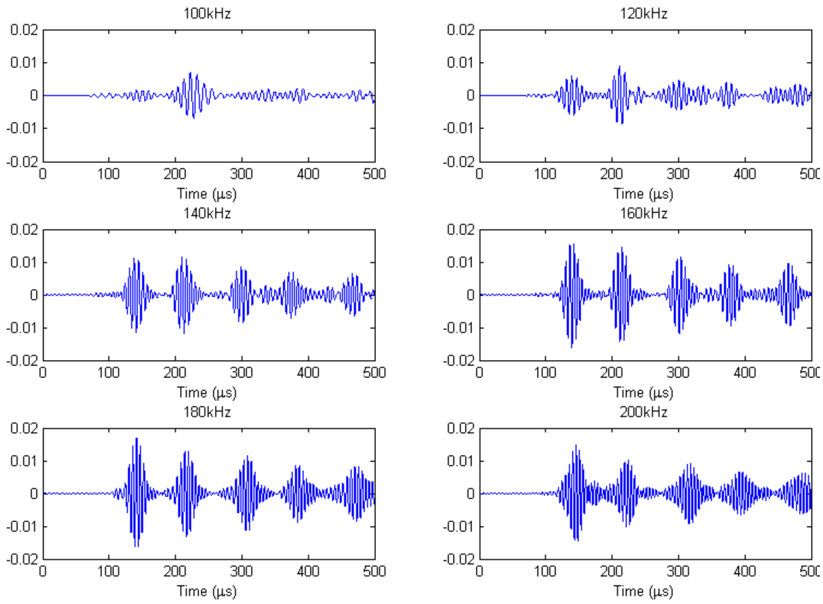

Figure 52: Different frequencies measurements. Three cycles, data filtered around centre frequency and 500 means.

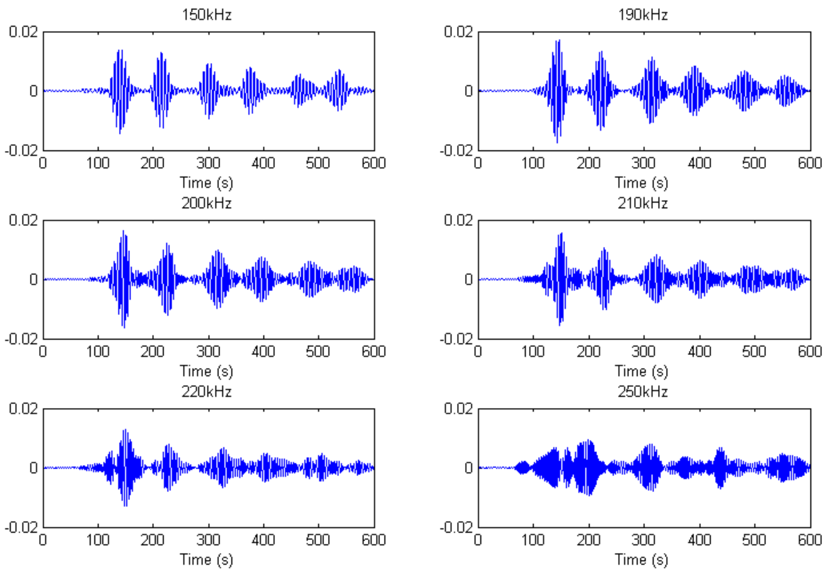

Figure 53: Different frequencies measurements. Three cycles, data filtered around centre frequency and 500 means.

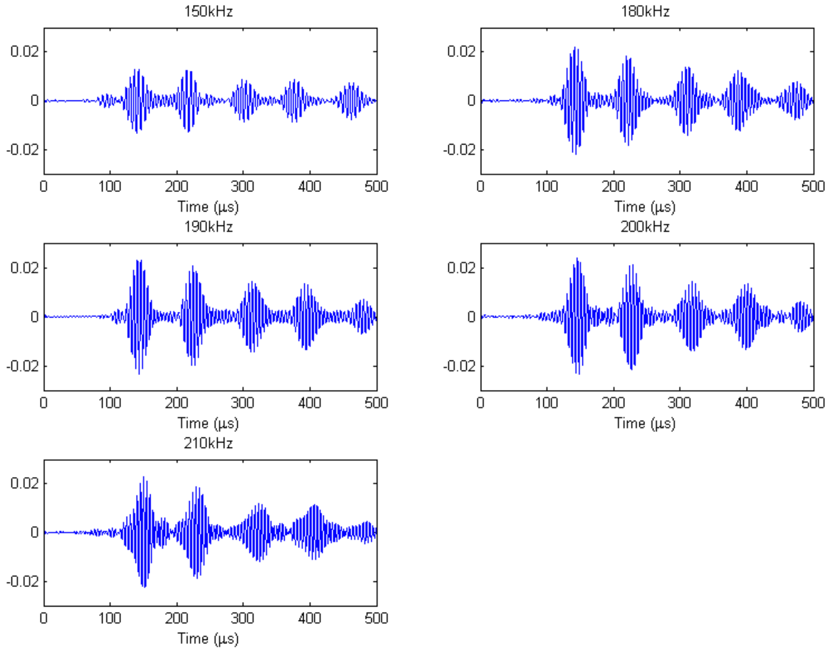

Figure 54: Different frequencies measurements. Three cycles, data filtered around centre frequency and 500 means.

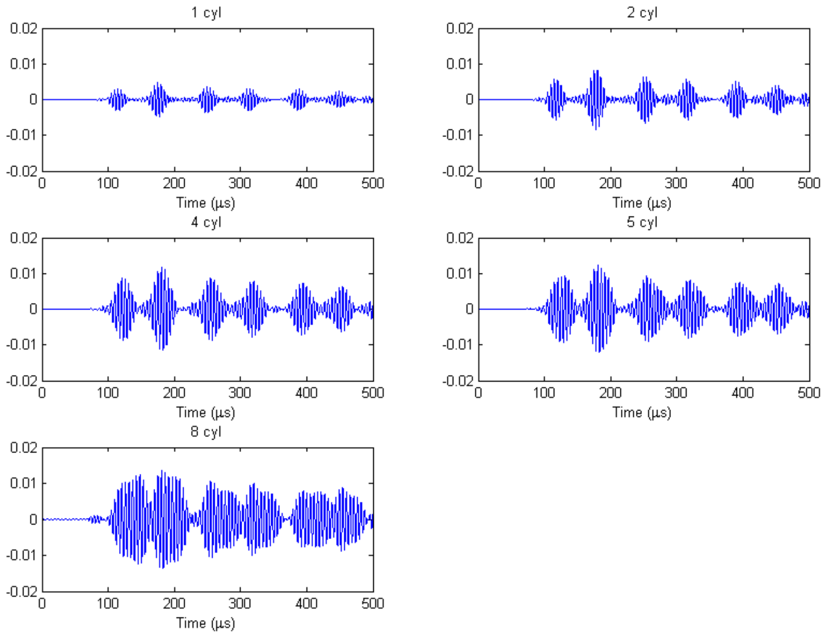

Figure 55: Different number of cycles measurements. Centre frequency of 200 kHz and 500 means.

11 Appendix D: Table of standard pipe sizes

Weights and Dimensions of Carbon Steel Pipe

Blue: Wall Thickness in Milimeters
Red: Weight Per Meter in Kilograms

PIPE SIZE	O.D. in mm	A.S.A. PIPE SCHEDULES													DBLE. E.H.
		5	10	20	30	40	STD	60	80	E.H.	100	120	140	160	
1/8"	10.287	.089 0.21	1.24 0.28			1.73 0.37	1.73 0.37		2.41 0.47	2.41 0.47					
1/4"	13.716	1.24 0.38	1.65 0.49			2.24 0.63	2.24 0.63		3.02 0.80	3.02 0.80					
3/8"	17.145	1.24 0.49	1.65 0.63			2.31 0.84	2.31 0.84		3.20 1.10	3.20 1.10					
1/2"	13.716	1.65 0.80	2.11 1.00			2.77 1.62	2.77 1.62		3.73 0.80	3.73 0.80				4.78 1.95	7.47 2.55
3/4"	26.670	1.65 1.03	2.11 1.28			2.87 1.69	2.87 1.69		3.91 2.20	3.91 2.20				5.56 2.90	7.82 3.64
1"	33.401	1.65 1.30	2.77 2.09			3.38 2.50	3.38 2.50		4.55 3.24	4.55 3.24				6.35 4.24	9.09 5.45
1-1/4"	42.164	1.65 1.65	2.77 2.70			3.56 3.39	3.56 3.39		4.85 4.47	4.85 4.47				6.35 5.61	9.70 7.77
1-1/2"	48.260	1.65 1.91	2.77 3.11			3.68 4.05	3.68 4.05		5.08 5.41	5.08 5.41				7.14 7.25	10.15 9.56
2"	60.325	1.65 2.40	2.77 3.93			3.91 5.44	3.91 5.44		5.54 7.48	5.54 7.48				8.74 11.11	11.07 13.44
2-1/2"	73.025	2.11 3.69	3.05 5.26			5.16 8.63	5.16 8.63		7.01 11.41	7.01 11.41				9.53 14.92	14.02 20.39
3"	88.900	2.11 4.51	3.05 6.45	3.96 8.29	4.78 9.92	5.49 11.29	5.49 11.29		7.62 15.27	7.62 15.27				11.13 21.35	15.24 27.68
3-1/2"	101.600	2.11 5.18	3.05 7.40			5.74 13.57	5.74 13.57		8.08 18.63	8.80 18.63					16.15 34.20
4"	114.300	2.11 5.84	3.05 8.36	4.78 12.91	5.56 14.91	6.02 16.07	6.02 16.07	7.14 18.87	8.56 22.32	8.56 22.32		11.13 28.32		13.49 33.54	17.12 41.03
5"	141.300	2.77 9.47	3.40 11.57	4.78 16.09	5.56 18.61	6.55 21.77	6.55 21.77	7.14 23.62	9.53 30.97	9.53 30.97		12.70 40.28		15.88 49.11	19.05 57.43
6"	168.275	2.77 11.32	3.40 13.84	4.78 19.27	6.35 25.38	7.11 28.26	7.11 28.26	9.53 37.31	10.97 42.56	10.97 42.56	12.70 48.73	14.27 54.20		18.26 67.56	21.95 79.22
8"	219.075	2.77 14.78	3.76 19.96	6.35 33.31	7.04 36.81	8.18 42.55	8.18 42.55	10.31 53.08	12.70 64.64	12.70 64.64	15.09 75.92	18.26 90.44	20.62 100.27	23.01 111.27	22.23 107.92
10"	273.050	3.40 22.63	4.19 27.78	6.35 41.77	7.80 51.03	9.27 60.31	9.27 60.31	12.70 81.55	15.09 96.01	12.70 81.55	18.26 114.75	21.44 133.06	25.40 155.15	28.58 172.33	25.40 155.15
12"	323.850	3.96 31.25	4.57 36.00	6.35 49.73	8.38 65.20	10.31 79.73	9.53 73.88	14.27 108.96	17.48 132.08	12.70 97.46	21.44 169.91	25.40 186.97	28.58 208.14	33.32 238.76	25.40 186.97
14"	355.600	3.96 34.36	6.35 54.69	7.92 67.90	9.53 81.33	11.13 94.55	9.53 81.33	15.09 126.71	19.05 158.10	12.70 107.39	23.83 194.96	27.79 224.65	31.75 253.56	35.71 281.70	
16"	406.400	4.19 41.56	6.35 62.64	7.92 77.83	9.53 93.27	12.70 123.30	9.53 93.27	16.66 160.12	21.44 203.53	12.70 123.30	26.19 245.66	30.96 286.64	36.53 333.19	40.49 365.35	
18"	457.200	4.19 46.81	6.35 70.57	7.92 87.71	11.13 122.38	14.27 155.80	9.53 105.16	19.05 205.74	23.83 254.55	12.70 139.15	29.36 309.62	34.93 363.56	39.67 408.26	45.24 459.37	
20"	508.000		6.35 78.55	9.53 117.15	12.70 155.12	15.09 183.42	9.53 117.15	20.62 247.83	26.19 311.17	12.70 155.12	32.54 381.53	38.10 441.49	44.45 508.11	50.01 564.81	
22"	558.800		6.35 86.54	9.53 129.13	12.70 171.09		9.53 129.13	22.23 294.25	28.58 373.83	12.70 171.09	34.93 451.42	41.28 527.02	47.63 600.63	53.98 672.26	
24"	609.600		6.35 94.53	9.53 141.12	14.27 209.64	17.48 255.41	9.53 141.12	24.61 355.26	30.96 442.08	12.70 187.06	38.89 547.71	46.02 640.03	52.37 720.15	59.54 808.22	
26"	660.400	6.35 102.36	7.92 127.36				9.53 152.87	10.31 165.18		12.70 202.72	14.27 227.23				
28"	711.200	6.35 110.34	7.92 137.32				9.53 164.85			12.70 218.69					
30"	762.000	6.35 118.31	7.92 147.28	12.70 234.67	15.88 292.18		9.53 176.84	10.31 191.11	11.13 206.09	12.70 234.67					
32"	812.800	6.35 126.31	7.92 157.24				9.53 188.82	10.31 204.08	11.13 220.08	12.70 250.64					
34"	863.600	6.35 134.30	7.92 167.20				9.53 200.31	10.31 217.05	11.13 234.08	12.70 266.61					
36"	914.400	6.35 142.13	7.92 176.96	12.70 282.27	15.88 351.70	19.05 420.42	9.53 212.56	10.31 229.76	11.13 247.31	12.70 282.27					
40"	1016.00						9.53 236.53			12.70 314.22					
42"	1066.80	7.92 207.92					9.53 248.52			12.70 330.19					
48"	1219.20						9.53 284.24			12.70 377.79					

Weights and Dimensions of Carbon Steel Pipe

Blue: Wall Thickness in Milimeters
Red: Weight Per Meter in Kilograms

Figure 56: Table of standard pipe sizes.[11]